5

DENSE MEDIA RADIATIVE TRANSFER THEORY FOR DENSE DISCRETE RANDOM MEDIA WITH PARTICLES OF MULTIPLE SIZES AND PERMITTIVITIES

L. Tsang

5.1 Introduction

In a dense medium, the particles occupy an appreciable fractional volume. In a nontenuous medium, the dielectric properties of the particles are substantially different from that of the background medium. The study of propagation and scattering of wave in dense nontenuous media have important applications in geophysical terrain and composite materials [1–12]. In the conventional radiative transfer theory, the particles are assumed to scatter independently [13–14]. Such an assumption is not valid for dense media and correlated scattering has to be taken into account. This has been confirmed by controlled laboratory experiment [5].

To study the propagation and scattering of waves in dense media, we have derived radiative transfer type equations from the Bethe–Salpeter equation under the ladder approximation [10–11,15]. These type of equations are similar in form to the conventional radiative transfer equations of independent scattering. We call them radiative wave equations or dense media radiative transfer equations to distinguish them from the conventional radiative transfer equations. Unlike the conventional theory which is derived heuristically, the dense media radiative transfer equation is derived from Dyson's equation under the quasicrystalline approximation with coherent potential (QCA–CP) and the Bethe–Salpeter equation under ladder approximation of correlated scatterers [10–11,15–16]. The dense media transfer equations take into account correlated scattering and correct the deficiencies of the conventional theory. The advantage of using QCA–CP in conjunction with ladder approximation is that the two approximations are consistent with energy conservation [9–10,17].

In our previous treatment of dense media transfer equations [10–11], the particles are assumed to be identical in size. In this paper, we consider dense discrete random media with multiple species of particles. The multiple species refers to the fact that the medium is a mixture of particles with different sizes and permittivities. This is particularly important because particles in geophysical terrain, composite and heterogeneous materials generally follow a size distribution and can also consist of different constituents. Recently, we have calculated effective propagation constant for such media [17–18]. In Section 5.2, we summarize the governing equations of Dyson's equation under QCA–CP approximation and the Bethe–Salpeter equation under ladder approximation for multiple species of particles that are correlated. Expressions

for the mass operator and the intensity operator are given. In Section 5.3, we calculate the effective propagation constants, mean Green's function and the mean field for a half-space discrete random medium of multiple species. In Section 5.4, we show the derivation of the dense media radiative transfer equations from the ladder approximation of correlated scatterers of multiple species. The pair distribution functions of multiple species are calculated by using the Percus–Yevick equation for non-interpenetrable spheres [19–25]. The final results of dense media radiative transfer equations for active and passive remote sensing are summarized respectively in Sections 5.5 and 5.6. All the four Stokes parameters are included so that the results are applicable to polarimetric remote sensing of dense media. The numerical results of dense media radiative transfer equations for active and passive remote sensing are illustrated in Section 5.7 for media with particles of multiple sizes and permittivities. The input physical parameters of the dense medium radiative transfer theory are the background medium permittivity, the particles permittivities and their size distributions. All other quantities are calculated. Given the input physical parameters, the pair distribution functions of particle positions and their Fourier transforms are calculated. Next, we calculate effective propagation constants, extinction rates, and albedo. Finally, the dense medium radiative transfer equations are solved to calculate bistatic scattering in active remote sensing and the brightness temperatures in passive remote sensing. Numerical results are also illustrated for the gamma size distributions. We also show that a medium consisting of a broad size distribution of particles tends to follow independent scattering more than a medium with narrow size distribution.

The propagation and scattering in dense discrete random media are studied in the context of microwave and optical remote sensing and communication. For such applications, one is generally interested in bistatic scattering characteristics of the scattering medium with appreciable albedo (say generally albedo larger than 0.01). For such media, the effective propagation constant $K = K_r + iK_i$ is complex. The imaginary part K_i, noted as coherent wave attenuation rate, is due to a combination of absorption and scattering. Thus it is nonzero even in cases when both the background and the particles are lossless. In order that albedo and scattering attenuation rate are both appreciable, two conditions must be obeyed. Firstly, one must not be in the ultra-low frequency limit when all the particles are extremely small compared to

the wavelength (say $ka < 0.01$ for all sizes in the particle size distribution). In such cases of ultra-low frequency, scattering attenuation rate and albedo are practically equal to zero. Secondly, the permittivity ϵ_{s_j} and fractional volume f_{s_j} of particle species s_j are such that if f_{s_j} is appreciable (say larger than 0.05), ϵ_{s_j} must be practically real with a imaginary part much less than the real part. If this is not obeyed, there will be a large fractional volume of lossy particles so that absorption dominates over scattering. Within these limits, we have found that QCA and QCA–CP generally give reasonable results and are in good agreement with experimental data [40] for both coherent wave attenuation rate and intensities of bistatic scattering.

5.2 Approximations of Mass and Intensity Operators for Dense Media with Multiple Species

Consider a discrete random medium consisting of discrete scatterers of L different species embedded in a background medium with permittivity ϵ (Fig. 5.1). The different species refers to the fact that particles can be of different shapes, sizes, and permittivities. However, interpenetration of particles is not allowed. The different species are denoted by $s_j = 1, 2, \ldots, L$. Each species of particles can have a distinct size, shape, and permittivity ϵ_{s_j}.

Electromagnetic waves propagation and scattering in a discrete random medium are governed by the Dyson's equation for the first moment and the Bethe–Salpeter equation for the second moment [27]. The coherent electric field $\langle \overline{E}(\overline{r}) \rangle$ satisfies the Dyson's equation

$$\overline{\nabla} \times \overline{\nabla} \times \langle \overline{E}(\overline{r}) \rangle - k^2 \langle \overline{E}(\overline{r}) \rangle = \int d\overline{r}' \overline{\overline{M}}(\overline{r}, \overline{r}') \cdot \langle \overline{E}(\overline{r}') \rangle \quad (1)$$

where $\overline{\overline{M}}$ is the mass operator. The mean dyadic Green's function $\left\langle \overline{\overline{G}}(\overline{r}, \overline{r}') \right\rangle$ obeys a similar equation

$$\overline{\nabla} \times \overline{\nabla} \times \left\langle \overline{\overline{G}}(\overline{r}, \overline{r}') \right\rangle - k^2 \left\langle \overline{\overline{G}}(\overline{r}, \overline{r}') \right\rangle = \overline{\overline{I}} \delta(\overline{r} - \overline{r}') + \int d\overline{r}'' \overline{\overline{M}}(\overline{r}, \overline{r}'') \cdot \left\langle \overline{\overline{G}}(\overline{r}'', \overline{r}') \right\rangle \quad (2)$$

We have used angular bracket <> to denote configurational average.

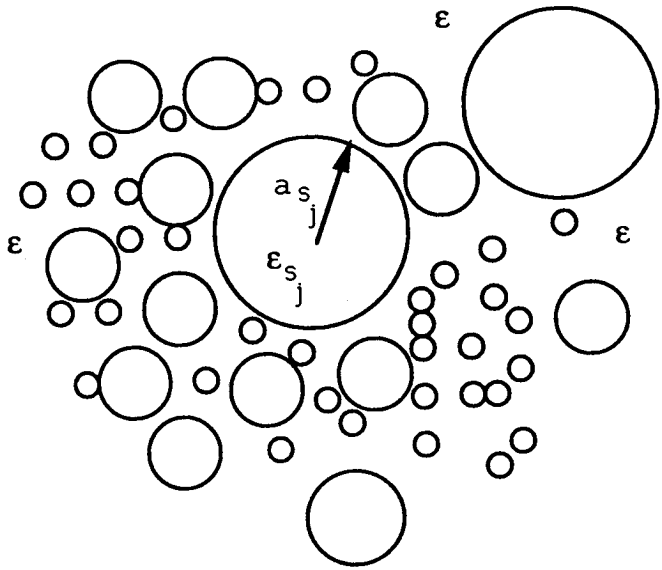

Figure 5.1 Discrete random medium consisting of particles of L different species, $s_j = 1, 2, \cdots, L$ with radius a_{s_j} and permittivity ϵ_{s_j} embedded in a background medium of permittivity ϵ.

The second moment of the field obeys the Bethe–Salpeter equation [27]

$$\begin{aligned}\langle E_\alpha(\bar{r}) E^*_\beta(\bar{r}')\rangle &= \langle E_\alpha(\bar{r})\rangle \langle E^*_\beta(\bar{r}')\rangle \\ &+ \sum_{\alpha',\beta'} \sum_{\alpha'',\beta''} \int d\bar{r}_1 \int d\bar{r}_2 \int d\bar{r}'_1 \int d\bar{r}'_2 \\ &\cdot \langle G_{\alpha\alpha'}(\bar{r},\bar{r}_1)\rangle \langle G^*_{\beta\beta'}(\bar{r}',\bar{r}'_1)\rangle I_{\alpha'\alpha''\beta'\beta''} \\ &(\bar{r}_1,\bar{r}_2;\bar{r}'_1,\bar{r}'_2) \langle E_{\alpha''}(\bar{r}_2) E^*_{\beta''}(\bar{r}'_2)\rangle \qquad (3)\end{aligned}$$

where $I_{\alpha'\alpha''\beta'\beta''}(\bar{r}_1,\bar{r}_2;\bar{r}'_1,\bar{r}'_2)$ is the intensity operator, superscript $*$ denotes complex conjugate and Greek index subscripts $\alpha,\beta = 1,2,3$ are used to denote the field components. Both the Dyson's equations (1)–(2), and the Bethe–Salpeter's equation (3) are exact. However the mass and intensity operators involve summation of infinite number of operators and approximations are needed to make the solution tractable. There is also a constraint of energy conservation on the ap-

proximations. Let $\overline{S}$ be the time-averaged Poynting's vector such that

$$\overline{S} = \frac{1}{4i\omega\mu}\left\{-\overline{E} \times \left(\overline{\nabla} \times \overline{E}^*\right) + \overline{E}^* \times \left(\overline{\nabla} \times \overline{E}\right)\right\} \tag{4}$$

where ω is angular frequency and μ is the permeability. Energy conservation requires that for the case of nonabsorptive background and scatterers when ϵ and ϵ_{s_j}, $j = 1, 2, \cdots, L$ are real, the integrated optical relation must be satisfied

$$\int d\overline{r}\ \left\langle \overline{\nabla} \cdot \overline{S} \right\rangle = 0 \tag{5}$$

Equation (5) is satisfied exactly for nonabsorptive background and scatterers if the mass and intensity operators are related by the following relationships [9,17]

$$M^*_{\alpha\beta}\left(\overline{r}, \overline{r}'\right) - M_{\beta\alpha}\left(\overline{r}', \overline{r}\right) + \sum_{\alpha',\beta'} \int d\overline{r}_1 \int d\overline{r}_2$$
$$\cdot \left[\left\langle G_{\alpha'\beta'}\left(\overline{r}_1, \overline{r}_2\right)\right\rangle - \left\langle G^*_{\beta'\alpha'}\left(\overline{r}_2, \overline{r}_1\right)\right\rangle\right] I_{\beta'\alpha\alpha'\beta}\left(\overline{r}_2, \overline{r}; \overline{r}_1, \overline{r}'\right) = 0 \tag{6}$$

where $M_{\alpha\beta}$ is the mass operator and $I_{\beta'\alpha\alpha'\beta}$ is the intensity operator. For the case of discrete random medium, relation (6) can be satisfied by using the quasicrystalline approximation with coherent potential (QCA–CP) [9,10,17] on the mass operator and the ladder approximation modified with pair distribution function for the intensity operator. For the case of multiple species of particles, the QCA–CP equations for the mass operator assume the following form [17–18]

$$\overline{\overline{t}}^{s_j}_j = \overline{\overline{U}}^{s_j}_j + \overline{\overline{U}}^{s_j}_j \left\langle \overline{\overline{G}} \right\rangle \overline{\overline{t}}^{s_j}_j \tag{7}$$

Equation (7) gives the equation for the transition operator $\overline{\overline{t}}^{s_j}_j$ of the j th particle of species s_j, in terms of the scattering potential, $\overline{\overline{U}}^{s_j}_j$, of the particle. This is basically the transition operator of the particle in the absence of other particles though the Green's function in (7) is that of the average Green's function.

$$\overline{\overline{C}}^{s_j}_j = \overline{\overline{t}}^{s_j}_j + \sum_{s_\ell=1}^{L} n_{s_\ell} \int d\overline{r}_\ell \overline{\overline{t}}^{s_j}_j \left\langle \overline{\overline{G}} \right\rangle h_{s_j s_\ell}\left(\overline{r}_j - \overline{r}_\ell\right) \overline{\overline{C}}^{s_\ell}_\ell \tag{8}$$

Equation (8) is the equation for the operator $\overline{\overline{C}}_j^{s_j}$ which can be interpreted as the transition operator of the j th particle of species s_j in the presence of other particles. The second term on the right hand side in (8) corresponds to the scattering from the ℓ th particle of species s_ℓ to the j th particle of species s_j. The scattering is averaged over number density n_{s_ℓ} and volume integration $d\overline{r}_\ell$ and weighted by $h_{s_j s_\ell}$ which is equal to the pair distribution function $g_{s_j s_\ell}$ minus 1.

$$\overline{\overline{M}} = \sum_{s_j=1}^{L} n_{s_j} \int d\overline{r}_j \, \overline{\overline{C}}_j^{s_j} \tag{9}$$

From (9), the mass operator is the sum of the transition operator $\overline{\overline{C}}_j^{s_j}$ averaged over number density n_{s_j} and volume integration $d\overline{r}_j$. The average Green's function obeys the equation

$$\left\langle \overline{\overline{G}} \right\rangle = \overline{\overline{G}}_o + \overline{\overline{G}}_o \overline{\overline{M}} \left\langle \overline{\overline{G}} \right\rangle \tag{10}$$

where n_{s_j} is the number of particles per unit volume of species s_j,

$$h_{s_j s_\ell}(\overline{r}) = g_{s_j s_\ell}(\overline{r}) - 1 \tag{11}$$

and $g_{s_j s_\ell}(\overline{r})$ is the pair distribution function of two particles of species s_j and s_ℓ separated by a distance $\overline{r}$. The multiple species pair functions can be computed by the Percus–Yevick approximation [22–23,17-18]. The function $h_{s_j s_\ell}(\overline{r})$ is generally nonzero over a range of a few particle diameters. This is because as $\overline{r} \to \infty$, $g_{s_j s_\ell} \to 1$ meaning that two particles are uncorrelated as their separation increases to infinity.

In (10), $\overline{\overline{G}}_o$ is the dyadic Green's operator with wavenumber $k = \omega\sqrt{\mu\epsilon}$ of the background medium. Equation (10) is the operator form of the integro-differential equation of (2).

The intensity operator that is energetically consistent with QCA–CP is that of the ladder approximation modified with pair distribution function as follows [17,27]

$$I_{\alpha\beta\alpha'\beta'}(\overline{r}, \overline{r}_1; \overline{r}', \overline{r}_1') = \sum_{s_j=1}^{L} \sum_{s_\ell=1}^{L} \int d\overline{r}_j \int d\overline{r}_\ell \left[n_{s_j} \delta_{s_j s_\ell} \delta(\overline{r}_j - \overline{r}_\ell) + n_{s_j} n_{s_\ell} h_{s_j s_\ell}(\overline{r}_j - \overline{r}_\ell) \right] C_{\ell\alpha\beta}^{s_\ell}(\overline{r}, \overline{r}_1) \, C_{j\alpha'\beta'}^{s_j *}(\overline{r}', \overline{r}_1') \tag{12}$$

where $C^{s_\ell}_{\ell\alpha\beta}$ is the $\alpha\beta$ component of $\overline{\overline{C}}^{s_\ell}_{\ell}$. In the usual ladder approximation for the discrete scatterers [27], the second term in the square bracket in (12) is absent which implies that the scatterers are uncorrelated. However, such correlation is important in dense medium and has been included in (12) for the intensity operator for dense media. Thus the ladder approximation essentially states that the second moment is a result of scattering by correlated scatterers with scattering $\overline{\overline{C}}^{s_\ell}$ and $\overline{\overline{C}}^{s_j}$ that are scattering matrices of the ℓth and jth scatterer in the presence of other scatterers.

The usual quasicrystalline approximation (QCA) consists of (7)–(10) with $\langle\overline{\overline{G}}\rangle$ in (7) and (8) (but not in (10)) replaced by the background propagator $\overline{\overline{G}}_o$ [9]. However, the usual QCA is not energetically consistent with ladder approximation. The QCA–CP version of (8) has the physical interpretation that in scattering from particle ℓ to particle j, the wave propagates with the effective medium propagator $\langle\overline{\overline{G}}\rangle$, while for QCA, the wave propagates with the background medium propagator $\overline{\overline{G}}_o$. Thus the QCA–CP approximation for discrete scatterers is analogous to that of nonlinear approximation for continuous random medium [27–29]. The coherent potential approximation for identical scatterers has been used in solid state physics problems [30–33].

The formulation in (1)–(12) is generally applicable to discrete random medium with particles of arbitrary size and shape. In the following sections, we shall study the solutions of the first and second moments equations for the case of small spherical particles in the Rayleigh limit with $ka_{s_j} \ll 1$, where a_{s_j} is the radius of the sphere of species s_j. Though the particles are small, the fractional volume $f_{s_j} = 4\pi n_{s_j} a^3_{s_j}/3$ remains appreciable.

5.3 Effective Propagation Constants, Mean Green's Function and Mean Field for Half Space Discrete Random Medium of Multiple Species

Consider a half-space of small spherical particles occupying the region $z < 0$ (Fig. 5.2). The upper and lower half-space are denoted as regions 0 and 1 respectively. The particles are dense and nontenuous so that the volume fraction $f_{s_j} = 4\pi n_{s_j} a^3_{s_j}/3$ of the s_j species can be ap-

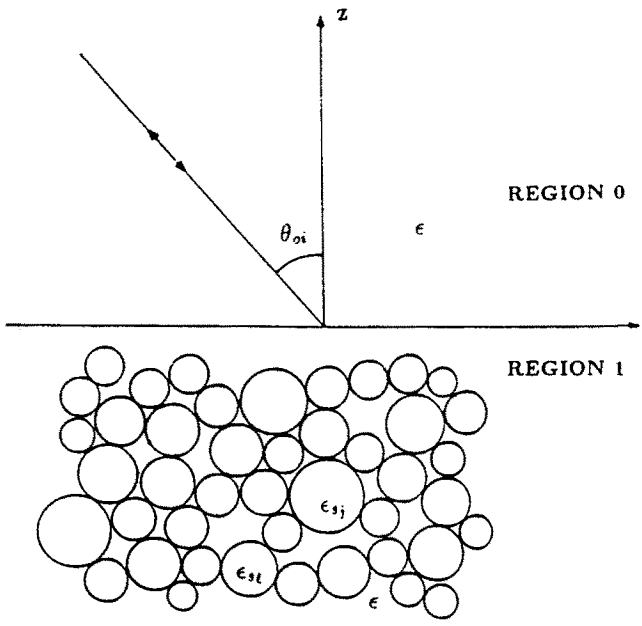

Figure 5.2 Active remote sensing with an incident electromagnetic wave impinging upon a half space discrete random medium of multiple species in the direction $(\pi - \theta_{oi}, \phi_i)$.

preciable and the wavenumber $k_{s_j} = \omega\sqrt{\mu\epsilon_{s_j}}$ of the particle of species s_j can be substantially different from the background wavenumber k. Hence, the effective propagation constant K in the lower half-space can be substantially different from k creating an effective boundary at $z = 0$. The mean Green's function and the mean field contain reflection terms due to this effective boundary. From (9)–(10), the half space mean Green's function obeys the equation

$$\left\langle \overline{\overline{G}}\left(\overline{r},\overline{r}'\right)\right\rangle = \overline{\overline{G}}_o\left(\overline{r},\overline{r}'\right) + \sum_{s_j=1}^{L} n_{s_j} \int d\overline{r}'' \int d\overline{r}''' \int_{z_j<0} d\overline{r}_j \overline{\overline{G}}_o\left(\overline{r},\overline{r}''\right) \overline{\overline{C}}_j^{s_j}\left(\overline{r}'',\overline{r}'''\right) \left\langle \overline{\overline{G}}\left(\overline{r}''',\overline{r}'\right)\right\rangle \quad (13)$$

where z_j is the z component of $\overline{r}_j$. To solve (13) in the small particles limit, we let the mean Green's function to be of the following form. For

$z,\ z' < 0$

$$\left\langle \overline{\overline{G}}\,(\bar{r},\bar{r}') \right\rangle = \overline{\overline{G}}_p\,(\bar{r},\bar{r}')\,\bar{r}'\,) + \overline{\overline{G}}_R\,(\bar{r},\bar{r}') \tag{14}$$

where

$$\overline{\overline{G}}_P\,(\bar{r},\bar{r}') = \left(\overline{\overline{I}} + \frac{1}{K^2}\overline{\nabla\nabla}\right) \frac{e^{iK|\bar{r}-\bar{r}'|}}{4\pi\,|\,\bar{r}-\bar{r}'\,|} \tag{15}$$

is the infinite space Green's function with effective propagation constant K. In (14) $\overline{\overline{G}}_R$ is the part of the Green's function that accounts for the boundary reflection term. Its form will be determined in subsequent discussion.

Next, we consider the solution of (7) and (8). We note that the scattering operator $\overline{\overline{U}}_j^{s_j}$ in the coordinate representation is

$$\left\langle \bar{r}\,|\,\overline{\overline{U}}_j^{s_j}\,|\,\bar{r}' \right\rangle = U^{s_j}\,(\bar{r}-\bar{r}_j)\,\overline{\overline{I}}\,\delta\,(\bar{r}-\bar{r}') \tag{16}$$

where

$$U^{s_j}\,(\bar{r}-\bar{r}_j) = \begin{cases} 0 & \text{for } |\,\bar{r}-\bar{r}_j\,| > a_{s_j} \\ k_{s_j}^2 - k^2 & \text{for } |\,\bar{r}-\bar{r}_j\,| \leq a_{s_j} \end{cases} \tag{17}$$

Because $ka_{s_j} \ll 1$, $\overline{\overline{U}}_j^{s_j}$ is short-ranged. Hence the transition operator $\overline{\overline{t}}_j^{s_j}$ is short-ranged. Thus, if $\bar{r}$ and $\bar{r}'$ are several diameters deep in the lower half-space, the contribution of $\overline{\overline{G}}_R$ in (11) will be much smaller than that of $\overline{\overline{G}}_P$. Hence, we have

$$\overline{\overline{t}}_j^{s_j} = \overline{\overline{U}}_j^{s_j} + \overline{\overline{U}}_j^{s_j}\,\overline{\overline{G}}_P\,\overline{\overline{t}}_j^{s_j} \tag{18}$$

Similar argument applies to (8), so that $\overline{\overline{C}}_j^{s_j}$ is also short-ranged, and it is nonzero in the vicinity of the particle located at $\bar{r}_j$ so that the boundary effect at $z=0$ can be ignored. Thus

$$\overline{\overline{C}}_j^{s_j} = \overline{\overline{t}}_j^{s_j} + \sum_{s_l=1}^{L} n_{s_l} \int d\bar{r}_l\,\overline{\overline{t}}_j^{s_j}\,\overline{\overline{G}}_P h_{s_j s_l}\,(\bar{r}_j - \bar{r}_l)\,\overline{\overline{C}}_l^{s_l} \tag{19}$$

Thus (18) and (19) for $\overline{\overline{t}}_j^{s_j}$ and $\overline{\overline{C}}_j^{s_j}$ become identical to that of the infinite space case which has been solved previously [17–18]. The solution for $\overline{\overline{t}}_j^{s_j}$ is, in momentum representation,

$$\left\langle \bar{p}\,|\,\overline{\overline{t}}^{s_j}\,|\,\bar{p}' \right\rangle = 3v_{s_j}K^2 y_{s_j}\left(1 + i\frac{2}{3}K^3 a_{s_j}^3 y_{s_j}\right)\overline{\overline{I}} \tag{20}$$

where $v_{s_j} = 4\pi a_{s_j}^3/3$ is the volume of the particle of s_j species and the function $y_{s_j}(K)$

$$y_{s_j}(K) = \frac{k_{s_j}^2 - k^2}{3K^2 + (k_{s_j}^2 - k^2)} \tag{21}$$

The solution for $\overline{\overline{C}}^{s_j}$, in momentum representation, is, in the small particles limit,

$$\left\langle \bar{p} \mid \overline{\overline{C}}^{s_j} \mid \bar{p}' \right\rangle = C_{s_j} \overline{\overline{I}} \tag{22}$$

where

$$C_{s_j} = \frac{3K^2 v_{s_j} y_{s_j}}{D(K)} \{ 1 + i\frac{2}{3} K^3 a_{s_j}^3 y_{s_j} + \frac{i2K^3}{3D(K)} \sum_{s_l=1}^{L} f_{s_l} y_{s_l} [y_{s_l} a_{s_l}^3 + \sum_{s_m=1}^{L} n_{s_m} y_{s_m} a_{s_m}^3 8\pi^3 H_{s_l s_m}(\bar{p}=0) + 6\pi^2 D(K) H_{s_j s_l}(\bar{p}=0)] \} \tag{23}$$

where the function $D(K)$

$$D(K) = 1 - \sum_{s_j=1}^{L} f_{s_j} y_{s_j} \tag{24}$$

$$H_{s_j s_l}(\bar{p}) = \frac{1}{(2\pi)^3} \int_{-\infty}^{\infty} d\bar{r} e^{i\bar{p}\cdot\bar{r}} h_{s_j s_l}(\bar{r}) \tag{25}$$

In solving (18) and (19), we have retained the leading term in the real part and the leading term in the imaginary part of $\overline{\overline{t}}_j^{s_j}$ and $\overline{\overline{C}}_j^{s_j}$. This enables us to keep track of the real part of the effective propagation constant and the effective attenuation rate. In the coordinate representation, we have

$$\overline{\overline{C}}_j^{s_j}(\bar{r}, \bar{r}') = C_{s_j} \delta(\bar{r} - \bar{r}_j) \delta(\bar{r}' - \bar{r}_j) \overline{\overline{I}} \tag{27}$$

Substituting (26) in (13) gives

$$\left\langle \overline{\overline{G}}(\bar{r}, \bar{r}') \right\rangle = \overline{\overline{G}}_o(\bar{r}, \bar{r}') + \sum_{s_j=1}^{L} n_{s_j} C_{s_j} \int_{z_j<0} d\bar{r}_j \, \overline{\overline{G}}_o(\bar{r}, \bar{r}_j) \left\langle \overline{\overline{G}}(\bar{r}_j, \bar{r}') \right\rangle \tag{27}$$

It can be recognized that (27) is the volume integral equation for a half-space Green's function with upper half-space wavenumber k and lower half-space wavenumber K if we identify in (27) that

$$\sum_{s_j=1}^{L} n_{s_j} C_{s_j} = K^2 - k^2 \tag{28}$$

From (23) and (28), after some algebraic manipulations, it follows that the effective propagation constant K is governed by the relation

$$K^2 = k^2 + \frac{3K^2}{D(K)} \sum_{s_l=1}^{L} f_{s_l} y_{s_l} \left\{ 1 + i \frac{2K^3}{3D(K)} \times \left[a_{s_l}^3 y_{s_l} + \sum_{s_j=1}^{L} y_{s_j} a_{s_j}^3 n_{s_j} 8\pi^3 H_{s_j s_l}(\bar{p}=0) \right] \right\} \tag{29}$$

We note that the effective propagation constant K as given by (29) is generally complex with the imaginary part accounting for the attenuation of the coherent wave due to both absorption and scattering. Generally, $K' \equiv \mathrm{Re}(K) \gg \mathrm{Im}(K) \equiv K''$. In view of (28), (27) becomes the standard volume integral equation for half-space Green's function [9]. The solution for $z,\ z' < 0$ is given by (14) with $\overline{\overline{G}}_P(\bar{r},\bar{r}')$ given by (15) and

$$\overline{\overline{G}}_R(\bar{r},\bar{r}') = \frac{i}{8\pi^2} \int_{-\infty}^{\infty} d\bar{k}_\perp \frac{e^{i\bar{k}_\perp \cdot (\bar{r}_\perp - \bar{r}'_\perp) - iK_z(z+z')}}{K_z} \cdot \left\{ R_e(\bar{k}_\perp) \hat{e}(-K_z) \hat{e}(K_z) + R_h(\bar{k}_\perp) \hat{h}(-K_z) \hat{h}(K_z) \right\} \tag{30}$$

where $\bar{k}_\perp = k_x \hat{x} + k_y \hat{y}$, $k_\perp = (k_x^2 + k_y^2)^{1/2}$, $K_z = (K^2 - k_\perp^2)^{1/2}$, $k_z = (k^2 - k_\perp^2)^{1/2}$, $\hat{e}$ and $\hat{h}$ are TE and TM unit vectors respectively with $\hat{e}(K_z) = (\hat{x}k_y - \hat{y}k_x)/k_\perp$ and $\hat{h}(K_z) = -K_z(\hat{x}k_x + \hat{y}k_y)/(Kk_\perp) + k_\perp \hat{z}/K$. The quantities R_e and R_h are TE and TM reflection coefficients respectively with

$$R_e(\bar{k}_\perp) = \frac{K_z - k_z}{K_z + k_z} \tag{31}$$

$$R_h(\bar{k}_\perp) = \frac{k^2 K_z - K^2 k_z}{k^2 K_z + K^2 k_z} \tag{32}$$

Similar expressions hold for $\left\langle \overline{\overline{G}}(\bar{r}, \bar{r}') \right\rangle$ for $\bar{r}$ in region 0 and $\bar{r}'$ in region 1.

Next, we calculate the coherent transmitted and reflected fields for an incident plane wave impinging from region 0 in the direction $(\pi - \theta_{oi},\ \phi_i)$ upon the lower half-space (Fig. 2). The incident electric field is

$$\overline{E}^{inc}(\bar{r}) = \left[E_{ih}\hat{h}(-k_{iz}) + E_{ie}\hat{e}(-k_{iz})\right] e^{ik_{ix}x + ik_{iy}y - ik_{iz}z} \tag{33}$$

where $k_{ix} = k \sin\theta_{oi} \cos\phi_i$, $k_{iy} = k \sin\theta_{oi} \sin\phi_i$, and $k_{iz} = k \cos\theta_{oi}$. From (1), (9), (26), and (28), it follows that for $\bar{r}$ in region 1, the coherent field obeys the equation

$$\begin{aligned} \overline{\nabla} \times \overline{\nabla} \times \left\langle \overline{E}(\bar{r}) \right\rangle &= k^2 \left\langle \overline{E}(\bar{r}) \right\rangle + \sum_{s_j=1}^{L} n_{s_j} C_{s_j} \left\langle \overline{E}(\bar{r}) \right\rangle \\ &= K^2 \left\langle \overline{E}(\bar{r}) \right\rangle \end{aligned} \tag{34}$$

which is the vector wave equation with wavenumber K. Hence, the coherent transmitted field in region 1 is [10]

$$\left\langle \overline{E}(\bar{r}) \right\rangle = \left[E_{ih}T_{ih}\hat{h}(-K_{iz}) + E_{ie}T_{ie}\hat{e}(-K_{iz})\right] e^{ik_{ix}x + ik_{iy}y - iK_{iz}z} \tag{35}$$

where $K_{iz} = (K^2 - k_{ix}^2 - k_{iy}^2)^{1/2}$, and

$$T_{ih} = \frac{2k_{iz}}{K\frac{k_{iz}}{k} + k\frac{K_{iz}}{K}} \tag{36}$$

$$T_{ie} = \frac{2k_{iz}}{K_{iz} + k_{iz}} \tag{37}$$

Similarly, for $\bar{r}$ in region 0, the coherent field is [10]

$$\begin{aligned} \left\langle \overline{E}(\bar{r}) \right\rangle = &\overline{E}^{inc}(\bar{r}) + e^{ik_{ix}x + ik_{iy}y + ik_{iz}z} \\ &\cdot \left\{ \hat{e}(k_{iz}) E_{ie} \frac{k_{iz} - K_{iz}}{k_{iz} + K_{iz}} + \hat{h}(k_{iz}) E_{ih} \frac{K^2 k_{iz} - k^2 K_{iz}}{K^2 k_{iz} + k^2 K_{iz}} \right\} \end{aligned} \tag{38}$$

The mean reflectivity for TE and TM waves are given respectively by the absolute squared of the mean reflection coefficient of (38).

5.4 Derivation of Dense Media Radiative Transfer Equation

In this section, we derived the dense media radiative transfer equation from ladder approximation of correlated scatterers. The basic physical idea is that because the particles are randomly distributed, the phases of the scattered fields are random so that the scattered fields generally average to zero except those terms that result in constructive interference. The mathematical approach is to identify and retain only the constructive interference terms in the ladder approximation and these terms combine to give the dense medium radiative transfer equation.

The second moment equation under ladder approximation is obtained by replacing the intensity operator in (3) by the expressions in (12) and (26). The intensity operator involves the product of the scattering operators. Thus, it is only necessary to retain the zeroth order solution of C_{s_j}. In (12) and (26), we then let

$$C_{s_j} \simeq C_{s_j}^{(0)} \tag{39}$$

where

$$C_{s_j}^{(0)} = \frac{3K^2 v_{s_j} y_{s_j}}{D} \tag{40}$$

The total electrical field can be decomposed into the coherent part $\langle \overline{E}(\bar{r}) \rangle$ and the incoherent part $\overline{\mathcal{E}}(\bar{r})$, so that

$$\overline{E}(\bar{r}) = \langle \overline{E}(\bar{r}) \rangle + \overline{\mathcal{E}}(\bar{r}) \tag{41}$$

Likewise, the second moment can also be decomposed into coherent and incoherent parts.

$$\langle E_\alpha(\bar{r}) E_\beta^*(\bar{r}') \rangle = \langle E_\alpha(\bar{r}) \rangle \langle E_\beta^*(\bar{r}') \rangle + \langle \mathcal{E}_\alpha(\bar{r}) \mathcal{E}_\beta^*(\bar{r}') \rangle \tag{42}$$

From (3), (12), (26), (39)–(42), it follows that the covariance of the incoherent field obeys the relation

$$\begin{aligned} &\langle \mathcal{E}_\alpha(\bar{r}) \mathcal{E}_\beta^*(\bar{r}') \rangle \\ &= \sum_{\alpha',\beta'} \int_{z_1<0} d\bar{r}_1 \int_{z_1'<0} d\bar{r}_1' \langle G_{\alpha\alpha'}(\bar{r},\bar{r}_1) \rangle \\ &\quad \cdot \langle G_{\beta\beta'}^*(\bar{r}',\bar{r}_1') \rangle Q(\bar{r}_1' - \bar{r}_1) \langle E_{\alpha'}(\bar{r}_1) E_{\beta'}^*(\bar{r}_1') \rangle \end{aligned} \tag{43}$$

where

$$Q(\bar{r}) = \sum_{s_j=1}^{L} \sum_{s_l=1}^{L} \left[n_{s_j} \delta_{s_j s_l} \delta(\bar{r}) + n_{s_j} n_{s_l} h_{s_j s_l}(\bar{r}) \right] C_{s_l}^{(0)} C_{s_j}^{(0)*} \tag{44}$$

The derivation of transport equation is in a manner analogous to that of continuous random medium [34–37]. From (43), it follows that the covariance of the incoherent field at $\bar{r}$ and $\bar{r}'$ comes from scattering at $\bar{r}_1$ and $\bar{r}_1'$ with $\bar{r}_1$ and $\bar{r}_1'$ integrated over the entire lower half-space. The major contributions do not come from $\bar{r}$ close to $\bar{r}_1$ nor $\bar{r}'$ close to $\bar{r}_1'$. Hence, the singularity of the Green's dyadic can be neglected in (43). The function $Q(\bar{r}_1' - \bar{r}_1)$ is short-ranged since it is only nonzero over a few particle diameters as dictated by the behavior of $h_{s_j s_l}(\bar{r})$. The rest of the integrand in (43) is varying on the wavelength scale. Since $ka_{s_j} \ll 1$, the function $Q(\bar{r}_1' - \bar{r}_1)$ is sharply peaked in the integrand of (43). Hence (43), in dyad form, can be approximated by

$$\left\langle \bar{\mathcal{E}}(\bar{r}) \bar{\mathcal{E}}^*(\bar{r}') \right\rangle = Q_o \int_{z_1<0} d\bar{r}_1 \left\langle \bar{\bar{G}}(\bar{r}, \bar{r}_1) \right\rangle \cdot \left\langle \bar{E}(\bar{r}_1) \bar{E}^*(\bar{r}_1) \right\rangle \cdot \left\langle \bar{\bar{G}}^{*t}(\bar{r}', \bar{r}_1) \right\rangle \tag{45}$$

where superscript t denotes transpose,

$$Q_o = \int_{-\infty}^{\infty} d\bar{r}\, Q(\bar{r}) = \frac{12\pi \mid K \mid^4}{\mid D \mid^2} \times \sum_{s_l=1}^{L} f_{s_l} y_{s_l} \left\{ a_{s_l}^3 y_{s_l}^* + \sum_{s_j=1}^{L} n_{s_j} a_{s_j}^3 y_{s_j}^* 8\pi^3 H_{s_j s_l}(\bar{p}=0) \right\} \tag{46}$$

The second equality in (46) is a result of using (44), (40) and (25). The quantity Q_o is real because $H_{s_j s_l} = H_{s_l s_j}$.

To solve (45), we can make a spectral decomposition of the incoherent field

$$\bar{\mathcal{E}}(\bar{r}) = \int_{-\infty}^{\infty} d\bar{k}_\perp e^{i\bar{k}_\perp \cdot \bar{r}_\perp} \left\{ \bar{\mathcal{E}}_u(z, \bar{k}_\perp) e^{iK_z' z} + \bar{\mathcal{E}}_d(z, \bar{k}_\perp) e^{-iK_z' z} \right\} \tag{47}$$

where $\bar{k}_\perp$ and $\bar{r}_\perp$ denote transverse wave vector and transverse coordinate vector respectively, $K_z' = \mathrm{Re}(K_z)$, $\bar{\mathcal{E}}_u(z, \bar{k}_\perp)$ is the upward

propagating incoherent envelope amplitude in transverse direction $\overline{k}_\perp$, and $\overline{\mathcal{E}}_d(z,\overline{k}_\perp)$ is the corresponding downward propagating envelope incoherent amplitude. Further decomposition can be made in terms of TM and TE waves.

$$\overline{\mathcal{E}}_u(z,\overline{k}_\perp) = \mathcal{E}_{hu}(z,\overline{k}_\perp)\,\hat{h}(K_z') + \mathcal{E}_{eu}(z,\overline{k}_\perp)\,\hat{e}(K_z') \tag{48}$$

$$\overline{\mathcal{E}}_d(z,\overline{k}_\perp) = \mathcal{E}_{hd}(z,\overline{k}_\perp)\,\hat{h}(-K_z') + \mathcal{E}_{ed}(z,\overline{k}_\perp)\,\hat{e}(-K_z') \tag{49}$$

Since we are mainly concerned with radiating waves, we have $K_z' \gg K_z''$, where $K_z'' = \mathrm{Im}(K_z)$, so that we can replace K_z in the argument of $\hat{h}$ and $\hat{e}$ by K_z'. In deriving the dense media radiative transfer equation, we distinguish two distance scales. The long distance scale is characterized by the mean free path ℓ_e, with $\ell_e = 1/(2K'')$, $K'' = \mathrm{Im}(K)$. The short distance scale is characterized by the wavelength scale $\lambda_e = 2\pi/K'$ with $K' = \mathrm{Re}(K)$. Transport type equations are derived based on the assumption that $\ell_e \gg \lambda$, $\ell_e \gg a_{s_j}$, i.e. the mean free path is much longer than the wavelength and the particle size. The condition is generally met for problems involving multiple scattering. Thus the envelope amplitude $\overline{\mathcal{E}}_u$ and $\overline{\mathcal{E}}_d$ in (48) and (49) are varying on the ℓ_e scale.

For z and z' separated on the λ_e scale, we assume that

$$\langle\, \overline{\mathcal{E}}_m(z,\overline{k}_\perp)\,\overline{\mathcal{E}}_n^*(z',\overline{k}_{\perp 1})\,\rangle = \delta(\overline{k}_\perp - \overline{k}_{\perp 1})\,\overline{\overline{\Lambda}}^{mn}(z,z';\overline{k}_\perp) \tag{50}$$

where $m,n = u,d$. The assumption of (50) is that incoherent fields with different transverse directions $\overline{k}_\perp$ of propagation are uncorrelated. For the same transverse direction, there is nonzero correlation. The upward and downward propagation waves with the same transverse $\overline{k}_\perp$ direction are correlated because of the effective reflecting interface at $z = 0$. This correlation is represented by $\overline{\overline{\Lambda}}^{ud}$. For $\overline{r} \neq \overline{r}'$, the mean Green's function of (14), (15)–(30) can be written in the form

$$\left\langle \overline{\overline{G}}(\overline{r},\overline{r}') \right\rangle = \int_{-\infty}^{\infty} d\overline{k}_\perp e^{i\overline{k}_\perp\cdot(\overline{r}_\perp - \overline{r}_\perp')} \left\{ \overline{\overline{g}}_P(\overline{k}_\perp,z,z') + \overline{\overline{g}}_R(\overline{k}_\perp,z,z') \right\} \tag{51}$$

where

$$\begin{aligned} \overline{\overline{g}}_P(\overline{k}_\perp,z,z') &= \overline{\overline{\sigma}}_>(K_z)\,e^{iK_z(z-z')} \qquad \text{for } z > z' \\ &= \overline{\overline{\sigma}}_<(K_z)\,e^{-iK_z(z-z')} \qquad \text{for } z < z' \end{aligned} \tag{52}$$

$$\overline{\overline{g}}_R(\overline{k}_\perp, z, z') = \overline{\overline{\sigma}}_R(K_z)\, e^{-iK_z(z+z')} \tag{53}$$

$$\overline{\overline{\sigma}}_>(K_z) = \frac{i}{8\pi^2 K_z}\left[\hat{e}(K_z)\,\hat{e}(K_z) + \hat{h}(K_z)\,\hat{h}(K_z)\right] \tag{54}$$

$$\overline{\overline{\sigma}}_<(K_z) = \frac{i}{8\pi^2 K_z}\left[\hat{e}(-K_z)\,\hat{e}(-K_z) + \hat{h}(-K_z)\,\hat{h}(-K_z)\right] \tag{55}$$

$$\begin{aligned}\overline{\overline{\sigma}}_R(K_z) = \frac{i}{8\pi^2 K_z}&\left[R_e(\overline{k}_\perp)\,\hat{e}(-K_z)\,\hat{e}(K_z)\right.\\ &\left.+ R_h(\overline{k}_\perp)\,\hat{h}(-K_z)\,\hat{h}(K_z)\right]\end{aligned} \tag{56}$$

Without loss of generality, let $z > z'$ in (45). Substituting (51)–(56) and (47)–(50) in (45), we obtain, after some algebraic manipulations,

$$\begin{aligned}&\overline{\overline{\Lambda}}^{uu}(z, z', \overline{k}_\perp)\, e^{iK_z'(z-z')} + \overline{\overline{\Lambda}}^{dd}(z, z', \overline{k}_\perp)\, e^{-iK_z'(z-z')}\\ &+ \overline{\overline{\Lambda}}^{ud}(z, z', \overline{k}_\perp)\, e^{iK_z'(z+z')} + \overline{\overline{\Lambda}}^{du}(z, z', \overline{k}_\perp)\, e^{-iK_z'(z+z')}\\ &= Q_o 4\pi^2 \Big\{ \int_{-\infty}^{z'} dz_1 \left[\overline{\overline{\sigma}}_>(K_z)\, e^{iK_z(z-z_1)} + \overline{\overline{\sigma}}_R(K_z)\, e^{-iK_z(z+z_1)}\right]\\ &\cdot \left[\overline{\overline{\lambda}}(K_{iz})\, e^{2K_{iz}'' z_1} + \langle\, \overline{\mathcal{E}}(\overline{r}_1)\, \overline{\mathcal{E}}^*(\overline{r}_1)\,\rangle\right]\\ &\cdot \left[\overline{\overline{\sigma}}_>^{*t}(K_z)\, e^{-iK_z^*(z'-z_1)} + \overline{\overline{\sigma}}_R^{*t}(K_z)\, e^{iK_z^*(z'+z_1)}\right]\\ &+ \int_{z'}^{z} dz_1 \left[\overline{\overline{\sigma}}_>(K_z)\, e^{iK_z(z-z_1)} + \overline{\overline{\sigma}}_R(K_z)\, e^{-iK_z(z+z_1)}\right]\\ &\cdot \left[\overline{\overline{\lambda}}(K_{iz})\, e^{2K_{iz}'' z_1} + \langle\, \overline{\mathcal{E}}(\overline{r}_1)\, \overline{\mathcal{E}}^*(\overline{r}_1)\,\rangle\right]\\ &\cdot \left[\overline{\overline{\sigma}}_<^{*t}(K_z)\, e^{iK_z^*(z'-z_1)} + \overline{\overline{\sigma}}_R^{*t}(K_z)\, e^{iK_z^*(z'+z_1)}\right]\\ &+ \int_{z}^{0} dz_1 \left[\overline{\overline{\sigma}}_<(K_z)\, e^{-iK_z(z-z_1)} + \overline{\overline{\sigma}}_R(K_z)\, e^{-iK_z(z+z_1)}\right]\\ &\cdot \left[\overline{\overline{\lambda}}(K_{iz})\, e^{2K_{iz}'' z_1} + \left\langle \overline{\mathcal{E}}(\overline{r}_1)\, \overline{\mathcal{E}}^*(\overline{r}_1)\right\rangle\right]\\ &\cdot \left[\overline{\overline{\sigma}}_<^{*t}(K_z)\, e^{iK_z^*(z'-z_1)} + \overline{\overline{\sigma}}_R^{*t}(K_z)\, e^{iK_z^*(z'+z_1)}\right]\Big\}\end{aligned} \tag{57}$$

where

$$\langle \overline{E}(\overline{r}_1)\rangle \left\langle \overline{E}^*(\overline{r}_1)\right\rangle = \overline{\overline{\lambda}}(K_{iz})\, e^{2K_{iz}'' z_1} \tag{58}$$

with

$$\begin{aligned}\overline{\overline{\lambda}}(K_{iz}) = &\left[E_{ih} T_{ih} \hat{h}(-K_{iz}) + E_{ie} T_{ie} \hat{e}(-K_{iz})\right]\\ &\left[E_{ih}^* T_{ih}^* \hat{h}(-K_{iz}) + E_{ie}^* T_{ie}^* \hat{e}(-K_{iz})\right]\end{aligned} \tag{59}$$

as the covariance of the coherent field. In (58), $K_{iz}'' = \mathrm{Im}(K_{iz})$. We first note that $\overline{\overline{\lambda}}(K_{iz})\exp(2K_{iz}''z_1) + \left\langle \overline{\mathcal{E}}(\overline{r}_1)\overline{\mathcal{E}}^*(\overline{r}_1)\right\rangle$ vary on the mean free path scale and do not vary on wavelength scale. The magnitudes of the various terms on the right hand side of (57) can be estimated. We distinguish between constructive interference terms and destructive interference terms. For example, a typical constructive interference term is

$$\int dz_1 e^{-iK_z(z-z_1)} e^{iK_z^*(z'-z_1)} = \mathcal{O}\left(\frac{1}{K_z''}\right) \tag{60}$$

where $\mathcal{O}$ represents of the order and $K_z'' = \mathrm{Im}(K_z)$. On the other hand, a typical destructive interference term is

$$\int dz_1 e^{-iK_z(z-z_1)+iK_z^*(z'+z_1)} = \mathcal{O}\left(\frac{1}{K_z'}\right) \tag{61}$$

where $K_z' = \mathrm{Re}(K_z)$. Generally, $K_z'' < K_z'$.

Terms of the type of (60) are of the constructive interference type as the phases of the integrand balance each other so that the integrand has little phase variation over the range of integration. Terms of the type of (61) are of the destructive interference type as the phases do not balance each other. Since $K_z' \gg K_z''$, terms of the destructive interference type are much smaller than that of the constructive interference type. Physically this corresponds to the fact that scattering due to products of fields travelling with different phases will average out to a small number after several wavelengths. We shall only retain terms of the constructive interference type. Using (47) and (50), we can calculate $\left\langle \overline{\mathcal{E}}(\overline{r}_1)\overline{\mathcal{E}}^*(\overline{r}_1)\right\rangle$ in the integrand of right hand side of (57) of which only constructive interference terms are retained. Thus, we can replace $\left\langle \overline{\mathcal{E}}(\overline{r}_1)\overline{\mathcal{E}}^*(\overline{r}_1)\right\rangle$ in the integrand of (57) by

$$\overline{\overline{J}}(z_1) = \int_{-\infty}^{\infty} d\overline{\gamma}_\perp \left\{ \overline{\overline{\Lambda}}^{uu}(z_1, z_1, \overline{\gamma}_\perp) + \overline{\overline{\Lambda}}^{dd}(z_1, z_1, \overline{\gamma}_\perp) \right\} \tag{62}$$

The next step is to balance terms on both sides of (57) that have the same phase dependence of z and z'. There are four types of phase dependence in (57): $\exp(iK_z'(z-z'))$, $\exp(-iK_z'(z-z'))$, $\exp(iK_z'(z+z'))$, and $\exp(-iK_z'(z+z'))$. We also let the separation of z and z' to be on the wavelength scale so that the contribution of $\int_{z'}^{z} dz_1$ in (57)

is small and can be neglected. Balancing terms with phase dependence $\exp(iK_z'(z-z'))$ gives

$$\overline{\overline{\Lambda}}^{uu}(z,z',\overline{k}_\perp)\,e^{iK_z'(z-z')} = 4\pi^2 Q_o e^{iK_z z - iK_z^* z'} \int_{-\infty}^{z'} dz_1 \overline{\overline{\sigma}}_>(K_z)\,e^{2K_z'' z_1} \cdot \left[\overline{\overline{\lambda}}(K_{iz})\,e^{2K_{iz}'' z_1} + \overline{\overline{J}}(z_1)\right] \cdot \overline{\overline{\sigma}}_>^{t*}(K_z) \tag{63}$$

Balancing $\exp(-iK_z'(z-z'))$, $\exp(iK_z'(z+z'))$, and $\exp(-iK_z'(z+z'))$ give three more equations similar to (63). Next we let z' approach z in (63) and in these three equations. From (63), we get

$$\begin{aligned}\overline{\overline{\Lambda}}^{uu}(z,z,\overline{k}_\perp) = 4\pi^2 Q_o \int_{-\infty}^{z} dz_1 \overline{\overline{\sigma}}_>(K_z)\,e^{-2K_z''(z-z_1)} \\ \cdot \left[\overline{\overline{\lambda}}(K_{iz})\,e^{2K_{iz}'' z_1}\right. \\ \left. + \overline{\overline{J}}(z_1)\right] \cdot \overline{\overline{\sigma}}_>^{t*}(K_z)\end{aligned} \tag{64}$$

From the other three equations, we get respectively

$$\begin{aligned}\overline{\overline{\Lambda}}^{dd}(z,z,\overline{k}_\perp) &= 4\pi^2 Q_o \int_{-\infty}^{z} dz_1 \overline{\overline{\sigma}}_R(K_z)\,e^{2K_z''(z+z_1)} \\ &\cdot \left[\overline{\overline{\lambda}}(K_{iz})\,e^{2K_{iz}'' z_1} + \overline{\overline{J}}(z_1)\right] \cdot \overline{\overline{\sigma}}_R^{t*}(K_z) \\ &+ 4\pi^2 Q_o \int_{z}^{0} dz_1 \left\{\overline{\overline{\sigma}}_<(K_z)\,e^{-2K_z''(z_1-z)}\right. \\ &\cdot \left[\overline{\overline{\lambda}}(K_{iz})\,e^{2K_{iz}'' z_1} + \overline{\overline{J}}(z_1)\right] \cdot \overline{\overline{\sigma}}_<^{*t}(K_z) \\ &+ \left.\overline{\overline{\sigma}}_R(K_z)\,e^{2K_z''(z+z_1)} \cdot \left[\overline{\overline{\lambda}}(K_{iz})\,e^{2K_{iz}'' z_1} + \overline{\overline{J}}(z_1)\right] \cdot \overline{\overline{\sigma}}_R^{*t}(K_z)\right\}\end{aligned} \tag{65}$$

$$\overline{\overline{\Lambda}}^{ud}(z,z,\overline{k}_\perp) = 4\pi^2 Q_o \int_{-\infty}^{z} dz_1\, \overline{\overline{\sigma}}_>(K_z)\,e^{2K_z'' z_1} \cdot \left[\overline{\overline{\lambda}}(K_{iz})\,e^{2K_{iz}'' z_1} + \overline{\overline{J}}(z_1)\right] \cdot \overline{\overline{\sigma}}_R^{t*}(K_z) \tag{66}$$

with the last one being just the complex conjugate and transpose of (66). Equations (64) to (66) are the integral equations for the covariance dyads. We note from (64) and (65) that $\overline{\overline{\Lambda}}^{uu}$ and $\overline{\overline{\Lambda}}^{dd}$ are functions of each other, while $\overline{\overline{\Lambda}}^{ud}$, the correlation between the upward

and downward waves with the same $\overline{k}_\perp$, is a function of $\overline{\overline{\Lambda}}^{uu}$ and $\overline{\overline{\Lambda}}^{dd}$ through (66). We can convert (64)–(66) into integro-differential equations with boundary conditions.

Differentiating (64), (65), and (66) gives respectively

$$\frac{d}{dz}\overline{\overline{\Lambda}}^{uu}(z,z,\overline{k}_\perp) = -2K_z''\overline{\overline{\Lambda}}^{uu}(z,z,\overline{k}_\perp)$$
$$+ 4\pi^2 Q_o \overline{\overline{\sigma}}_>(K_z)\cdot\left[\overline{\overline{\lambda}}(K_{iz})\,e^{2K_{iz}''z} + \overline{\overline{J}}(z)\right]\cdot\overline{\overline{\sigma}}_>^{t*}(K_z) \tag{67}$$

$$\frac{d}{dz}\overline{\overline{\Lambda}}^{dd}(z,z,\overline{k}_\perp) = 2K_z''\overline{\overline{\Lambda}}^{dd}(z,z,\overline{k}_\perp)$$
$$- 4\pi^2 Q_o \overline{\overline{\sigma}}_<(K_z)\cdot\left[\overline{\overline{\lambda}}(K_{iz})\,e^{2K_{iz}''z} + \overline{\overline{J}}(z)\right]\cdot\overline{\overline{\sigma}}_<^{*t}(K_z) \tag{68}$$

$$\frac{d}{dz}\overline{\overline{\Lambda}}^{ud}(z,z,\overline{k}_\perp) = 2K_z''\overline{\overline{\Lambda}}^{ud}(z,z,\overline{k}_\perp)$$
$$+ 4\pi^2 Q_o \overline{\overline{\sigma}}_>(K_z)\,e^{2K_z''z}\cdot\left[\overline{\overline{\lambda}}(K_{iz})\,e^{2K_{iz}''z} + \overline{\overline{J}}(z)\right]\cdot\overline{\overline{\sigma}}_R^{t*}(K_z) \tag{69}$$

The boundary condition for the integro-differential equation of (67)–(69) can be obtained by setting $z = 0$ in the integral equations of (64)–(65) which gives

$$\overline{\overline{\Lambda}}^{dd}(z,z,\overline{k}_\perp)\Big|_{z=0} = \overline{\overline{R}}_c(K_z)\cdot\overline{\overline{\Lambda}}^{uu}(z,z,\overline{k}_\perp)\Big|_{z=0}\cdot\overline{\overline{R}}_c^{t*}(K_z) \tag{70}$$

where

$$\overline{\overline{R}}_c(K_z) = R_e(\overline{k}_\perp)\,\hat{e}(-K_z)\,\hat{e}(K_z) + R_h(\overline{k}_\perp)\,\hat{h}(-K_z)\,\hat{h}(K_z) \tag{71}$$

Equations (67)–(68) and (70)–(71) are the transport equations for the covariance dyads. They are in the form that resemble the radiative transfer equations. They can be cast into the more standard form in terms of angular direction (θ,ϕ). Transformation from $\overline{k}_\perp$ to angular direction (θ,ϕ) is done by setting $\overline{k}_\perp = k_x\hat{x} + k_y\hat{y}$, $k_x = K'\sin\theta\cos\phi$, and $k_y = K'\sin\theta\sin\phi$. Also we have $\int_{-\infty}^{\infty} d\overline{k}_\perp \simeq \int_0^{\pi/2} d\theta\sin\theta\cos\theta \int_0^{2\pi} d\phi K'^2$. Only the radiating waves can contribute to constructive interference terms. Constructive interference terms arise from scattering from waves integrated over a sizable region of many wavelengths and evanescent waves do not fall into that category. We can put (67)–(68) in 2×2 matrix form.

Let $\Lambda_{11}^{uu}(z,z,\bar{k}_\perp)$, $\Lambda_{12}^{uu}(z,z,\bar{k}_\perp)$, $\Lambda_{21}^{uu}(z,z,\bar{k}_\perp)$ and $\Lambda_{22}^{uu}(z,z,\bar{k}_\perp)$ be the $\hat{h}\hat{h}$, $\hat{h}\hat{e}$, $\hat{e}\hat{h}$, and $\hat{e}\hat{e}$ components of $\overline{\overline{\Lambda}}^{uu}(z,z,\bar{k}_\perp)$ respectively. That is $\Lambda_{12}^{uu}(z,z,\bar{k}_\perp) = \hat{h}(K_z') \cdot \overline{\overline{\Lambda}}^{uu}(z,z,\bar{k}_\perp) \cdot \hat{e}(K_z')$ etc. Similar definitions apply to $\Lambda_{ij}^{dd}(z,z,\bar{k}_\perp)$ with $i,j = 1,2$. For $0 \le \theta < \pi/2$, $0 \le \phi < 2\pi$, the 2×2 matrices be defined by

$$\underline{\underline{\Lambda}}^{uu}(z,z,\bar{k}_\perp) = \begin{bmatrix} \Lambda_{11}^{uu}(z,z,\bar{k}_\perp) & \Lambda_{12}^{uu}(z,z,\bar{k}_\perp) \\ \Lambda_{21}^{uu}(z,z,\bar{k}_\perp) & \Lambda_{22}^{uu}(z,z,\bar{k}_\perp) \end{bmatrix} = \underline{\underline{\Lambda}}(z,\theta,\phi) \tag{72}$$

$$\underline{\underline{\Lambda}}^{dd}(z,z,\bar{k}_\perp) = \begin{bmatrix} \Lambda_{11}^{dd}(z,z,\bar{k}_\perp) & \Lambda_{12}^{dd}(z,z,\bar{k}_\perp) \\ \Lambda_{21}^{dd}(z,z,\bar{k}_\perp) & \Lambda_{22}^{dd}(z,z,\bar{k}_\perp) \end{bmatrix} = \underline{\underline{\Lambda}}(z,\pi-\theta,\phi) \tag{73}$$

For $0 < \theta < \pi/2$, $0 < \phi < 2\pi$, let

$$\underline{\underline{F}}(K_z', K_{z\gamma}') = \begin{bmatrix} f_{11}(K_z', K_{z\gamma}') & f_{12}(K_z', K_{z\gamma}') \\ f_{21}(K_z', K_{z\gamma}') & f_{22}(K_z', K_{z\gamma}') \end{bmatrix} = \underline{\underline{F}}(\theta,\phi;\theta_\gamma,\phi_\gamma) \tag{74}$$

where $K_{z\gamma} = (K^2 - \gamma_\perp^2)^{1/2}$, $K_{z\gamma}' = \mathrm{Re}(K_{z\gamma})$,

$$f_{11}(K_z', K_{z\gamma}') = \hat{h}(K_z') \cdot \hat{h}(K_{z\gamma}') \tag{75}$$

$$f_{12}(K_z', K_{z\gamma}') = \hat{h}(K_z') \cdot \hat{e}(K_{z\gamma}') \tag{76}$$

$$f_{21}(K_z', K_{z\gamma}') = \hat{e}(K_z') \cdot \hat{h}(K_{z\gamma}') \tag{77}$$

$$f_{22}(K_z', K_{z\gamma}') = \hat{e}(K_z') \cdot \hat{e}(K_{z\gamma}') \tag{78}$$

Also

$$\underline{\underline{F}}(-K_z', K_{z\gamma}') = F(\pi-\theta,\phi;\theta_\gamma,\phi_\gamma) \tag{79}$$

etc. Then, (67) and (68) assume the following matrix form respectively.

$$\begin{aligned} \frac{d}{dz}\underline{\underline{\Lambda}}(z,\theta,\phi) &= -\kappa_e \sec\theta \underline{\underline{\Lambda}}(z,\theta,\phi) \\ &+ \frac{Q_o \sec^2\theta}{16\pi^2 K'^2} \underline{\underline{F}}(\theta,\phi;\pi-\theta_i,\phi_i) \cdot \underline{\underline{\lambda}}(K_{iz}) \cdot \underline{\underline{F}}(\pi-\theta_i,\phi_i;\theta,\phi)\, e^{\kappa_e z \sec\theta_i} \\ &+ \frac{Q_o \sec^2\theta}{16\pi^2} \int_0^\pi d\theta_\gamma \sin\theta_\gamma \mid \cos\theta_\gamma \mid \int_0^{2\pi} d\phi_\gamma \{\underline{\underline{F}}(\theta,\phi;\theta_\gamma,\phi_\gamma) \\ &\cdot \underline{\underline{\Lambda}}(z,\theta_\gamma,\phi_\gamma) \cdot \underline{\underline{F}}(\theta_\gamma,\phi_\gamma;\theta,\phi)\} \end{aligned} \tag{80}$$

$$\frac{d}{dz}\underline{\underline{\Lambda}}(z,\pi-\theta,\phi) = \kappa_e \sec\theta \underline{\underline{\Lambda}}(z,\pi-\theta,\phi)$$
$$- \frac{Q_o \sec^2\theta}{16\pi^2 K'^2}\underline{\underline{F}}(\pi-\theta,\phi;\pi-\theta_i,\phi_i)$$
$$\cdot \underline{\underline{\lambda}}(K_{iz}) \cdot \underline{\underline{F}}(\pi-\theta_i,\phi_i;\pi-\theta,\phi)\, e^{\kappa_e z \sec\theta_i}$$
$$- \frac{Q_o \sec^2\theta}{16\pi^2}\int_0^{\pi} d\theta_\gamma \sin\theta_\gamma \mid \cos\theta_\gamma \mid$$
$$\times \int_0^{2\pi} d\phi_\gamma \{\underline{\underline{F}}(\pi-\theta,\phi;\theta_\gamma,\phi_\gamma)$$
$$\cdot \underline{\underline{\Lambda}}(z,\theta_\gamma,\phi_\gamma) \cdot \underline{\underline{F}}(\theta_\gamma,\phi_\gamma;\pi-\theta,\phi)\} \tag{81}$$

where

$$\kappa_e = 2K'' \tag{82}$$

is the extinction rate,

$$\underline{\underline{\lambda}}(K_{iz}) = \begin{bmatrix} |E_{ih}|^2 |T_{ih}|^2 & E_{ih}E_{ie}^* T_{ih}T_{ie}^* \\ E_{ie}E_{ih}^* T_{ie}T_{ih}^* & |E_{ie}|^2 |T_{ie}|^2 \end{bmatrix} \tag{83}$$

$K'_{iz} = K' \sin\theta_i$, and θ_i and θ_{oi} are related by Snell's law $\theta_i = \sin^{-1}(k \sin\theta_{oi}/K')$. In deriving (80) and (81), we have also made use of the property that $K''_z = K'' \sec\theta$. Equations (80)–(81) are the radiative transfer equations for the field covariance matrix $\underline{\underline{\Lambda}}(z,\theta,\phi)$. The boundary condition is obtained from (70)–(73), and is, for $0 \leq \theta < \pi/2$, $0 \leq \phi < 2\pi$

$$\underline{\underline{\Lambda}}(z=0,\pi-\theta,\phi) =$$
$$\begin{bmatrix} |R_h(\bar{k}_\perp)|^2 \Lambda_{11}(z=0,\theta,\phi) & R_h(\bar{k}_\perp)R_e^*(\bar{k}_\perp)\Lambda_{12}(z=0,\theta,\phi) \\ R_h^*(\bar{k}_\perp)R_e(\bar{k}_\perp)\Lambda_{21}(z=0,\theta,\phi) & |R_e(\bar{k}_\perp)|^2 \Lambda_{22}(z=0,\theta,\phi) \end{bmatrix} \tag{84}$$

Equations (80)–(84) can be put in the standard form involving Stokes parameters by defining

$$\mathcal{I}_1(z,\theta,\phi) = \frac{K'^3}{k} \mid \cos\theta \mid \Lambda_{11}(z,\theta,\phi) \tag{85}$$

$$\mathcal{I}_2(z,\theta,\phi) = \frac{K'^3}{k} \mid \cos\theta \mid \Lambda_{22}(z,\theta,\phi) \tag{86}$$

$$\mathcal{I}_3(z,\theta,\phi) = -2\frac{K'^3}{k} \mid \cos\theta \mid \mathrm{Re}\,(\Lambda_{21}(z,\theta,\phi)) \tag{87}$$

$$\mathcal{I}_4(z,\theta,\phi) = -2\frac{K'^3}{k} \mid \cos\theta \mid \mathrm{Im}\,(\Lambda_{21}(z,\theta,\phi)) \tag{88}$$

and the 4×1 Stokes vector is

$$\underline{\mathcal{I}}(z,\theta,\phi) = \begin{bmatrix} \mathcal{I}_1(z,\theta,\phi) \\ \mathcal{I}_2(z,\theta,\phi) \\ \mathcal{I}_3(z,\theta,\phi) \\ \mathcal{I}_4(z,\theta,\phi) \end{bmatrix} \tag{89}$$

The albedo will then be

$$\tilde{\omega} = \frac{Q_o}{6\pi\kappa_e} \tag{90}$$

with Q_o as given by (46). The scattering coupling coefficients for Stokes parameters are the phase matrix elements, which, in view of (80)–(81), can be expressed in terms of products of $\underline{\underline{F}}(\theta,\phi;\theta_\gamma,\phi_\gamma)$ elements. The result radiative transfer equation for the Stokes parameters and the phase matrix elements are summarized in Sections 5.5 and 5.6 respectively for active and passive microwave remote sensing.

5.5 Dense Media Radiative Transfer Equations for Active Remote Sensing

In this section, we summarize the key equations concerning the dense media radiative transfer equation as derived in Section 5.2 to 5.4 for active remote sensing (Fig. 5.2). The incident electromagnetic wave is in the direction $(\pi - \theta_{oi}, \phi_i)$. The incident electric field is given by equation (33) with E_{ih} and E_{ie} being the amplitudes of TM and TE wave respectively.

As shown in Section 5.2–5.3, the spherical particle in the medium are characterized by L species, $s_j = 1,2,\ldots,L$, with each species s_j having the radius a_{s_j}, permittivity ϵ_{s_j} and fractional volume $f_{s_j} = 4\pi n_{s_j} a_{s_j}^3/3$ where n_{s_j} is the number density of the s_j species. The particles are embedded in a background medium with permittivity ϵ. The dense media radiative transfer equations have been derived for the case of small particles assuming $ka_{s_j} \ll 1$ where k is the wavenumber of the background medium.

a. Step 1: Effective Propagation Constants, Extinction Rates, and Coherent Transmitted Wave.

As shown in Section 5.3, the lower half-space of region 1 can be represented by an effective propagation constant K, where K obeys

the equation

$$\begin{aligned} K^2 \approx & K'^2 + i2K'K'' \\ = & k^2 + \frac{3K_o^2}{D(K_o)} \sum_{s_\ell=1}^{L} f_{s_\ell} y_{s_\ell}(K_o) \\ & \times \left\{ 1 + i\frac{2K_o^3}{3D(K_o)} \left[a_{s_\ell}^3 y_{s_\ell}(K_o) + \sum_{s_j=1}^{L} y_{s_j}(K_o) \right. \right. \\ & \left. \left. \times a_{s_j}^3 n_{s_j} 8\pi^3 H_{s_j s_\ell}(p=0) \right] \right\} \end{aligned} \tag{91}$$

where K_o^2 represents zeroth order solution and satisfies the following equation

$$K_o^2 = k^2 + \frac{3K_o^2}{D(K_o)} \sum_{s_\ell=1}^{L} f_{s_\ell} y_{s_\ell}(K_o) \tag{92}$$

and

$$D(K_o) = 1 - \sum_{s_j=1}^{L} f_{s_j} y_{s_j}(K_o) \tag{93}$$

$$y_{s_j}(K_o) = \frac{k_{s_j}^2 - k^2}{3K_o^2 + (k_{s_j}^2 - k^2)} \tag{94}$$

The quantities $H_{s_\ell s_j}$ $(\overline{p} = 0)$ are related to the Fourier transform of the pair functions as given by (11) and (25). The computation of these quantities for non-interpenetrable spheres of L species have been reported [19–25, 17–18]. To calculate numerical results of the nonlinear equation of K in (91), we solve (92) first for K_o. Equation (92) with (93)–(94) is a polynomial equation for K_o and only one solution has the correct physical meaning of effective propagation constant. That solution is then substituted back in (91) to calculate K. The extinction rate is $\kappa_e = 2K''$ where $K'' = \mathrm{Im}(K)$. Snell's law can then be applied so that the transmitted angle of the coherent wave is $\theta_i = \sin^{-1}(k \sin\theta_{oi}/K')$ where $K' = \mathrm{Re}(K)$. The coherent transmission wave amplitude for TM and TE waves are given respectively by (36)–(37) with $k_{iz} = k\cos\theta_{oi}$ and $K_{iz} = (K^2 - k^2 \sin^2\theta_{oi})^{1/2}$.

b. Step 2: Dense Media Radiative Transfer Equation for the Incoherent Wave.

By using the definitions of Stokes parameters of (89), (85)–(88) in (80)–(83), it follows after some algebraic manipulations that the dense media radiative transfer equations for the incoherent 4×1 Stokes vector $\underline{I}(z, \theta, \phi)$ in region 1 is, for $0 \leq \theta \leq \pi$, and $0 \leq \phi < 2\pi$,

$$\cos\theta \frac{d}{dz}\underline{I}(z,\theta,\phi) - \kappa_e \underline{I}(z,\theta,\phi) + \frac{\kappa_e \tilde{\omega}}{4\pi}\frac{K'}{k}\underline{\underline{P}}(\theta,\phi;\pi-\theta_i,\phi_i)\underline{\lambda}(K_{iz}) \times e^{\kappa_e z \sec\theta_i} + \frac{\kappa_e\tilde{\omega}}{4\pi}\int_0^{\pi} d\theta_\gamma \sin\theta_\gamma \int_0^{2\pi} d\phi_\gamma \underline{\underline{P}}(\theta,\phi;\theta_\gamma,\phi_\gamma)\underline{I}(z,\theta_\gamma,\phi_\gamma) \tag{95}$$

where $\tilde{\omega}$ is, from (46) and (90)

$$\tilde{\omega} = \frac{2|K_o|^4}{\kappa_e |D(K_o)|^2} \sum_{s_\ell=1}^{L} f_{s_\ell} y_{s_\ell}(K_o)\Big\{ a_{s_\ell}^3 y_{s_\ell}^*(K_o) + \sum_{s_j=1}^{L} n_{s_j} a_{s_j}^3 y_{s_j}^*(K_o) 8\pi^3 H_{s_j s_\ell}(\bar{p}=0)\Big\} \tag{96}$$

In (95), the coherent transmitted Stokes vector, $\underline{\lambda}(K_{iz})$ is

$$\underline{\lambda}(K_{iz}) = \begin{bmatrix} T_{ih}^2 \mid E_{ih} \mid^2 \\ T_{ie}^2 \mid E_{ie} \mid^2 \\ -2T_{ie}T_{ih}\mathrm{Re}(E_{ih}^* E_{ie}) \\ -2T_{ie}T_{ih}\mathrm{Im}(E_{ih}^* E_{ie}) \end{bmatrix} \tag{97}$$

where T_{ih} and T_{ie} are as given (36) and (37), both of which are practically real since $K_{iz}'' \ll K_{iz}'$, and for convenience, we shall just take their respective real parts when calculating (97). The second term in (95) is the source term for the incoherent wave and corresponds to a single scattering of the coherent wave into incoherent wave. The elements of the 4×4 phase matrix $\underline{\underline{P}}(\theta, \phi; \theta_\gamma, \phi_\gamma)$ are, from (80)–(89)

$$P_{11}(\theta,\phi;\theta_\gamma,\phi_\gamma) = \frac{3}{2}[\sin\theta\sin\theta_\gamma + \cos\theta\cos\theta_\gamma\cos(\phi-\phi_\gamma)]^2 \tag{98}$$

$$P_{12}(\theta,\phi;\theta_\gamma,\phi_\gamma) = \frac{3}{2}\cos^2\theta\sin^2(\phi-\phi_\gamma) \tag{99}$$

$$P_{13}(\theta,\phi;\theta_\gamma,\phi_\gamma) = -\frac{3}{2}[\sin\theta\sin\theta_\gamma + \cos\theta\cos\theta_\gamma\cos(\phi-\phi_\gamma)]\cos\theta\sin(\phi-\phi_\gamma) \tag{100}$$

$$P_{21}(\theta,\phi;\theta_\gamma,\phi_\gamma) = \frac{3}{2}\cos^2\theta_\gamma\sin^2(\phi-\phi_\gamma) \tag{101}$$

$$P_{22}(\theta,\phi;\theta_\gamma,\phi_\gamma) = \frac{3}{2}\cos^2(\phi-\phi_\gamma) \tag{102}$$

$$P_{23}(\theta,\phi;\theta_\gamma,\phi_\gamma) = \frac{3}{2}\cos\theta_\gamma\sin(\phi-\phi_\gamma)\cos(\phi-\phi_\gamma) \tag{103}$$

$$P_{31}(\theta,\phi;\theta_\gamma,\phi_\gamma) = 3\cos\theta_\gamma\sin(\phi-\phi_\gamma)[\sin\theta\sin\theta_\gamma + \cos\theta\cos\theta_\gamma\cos(\phi-\phi_\gamma)] \tag{104}$$

$$P_{32}(\theta,\phi;\theta_\gamma,\phi_\gamma) = -3\cos\theta\cos(\phi-\phi_\gamma)\sin(\phi-\phi_\gamma) \tag{105}$$

$$P_{33}(\theta,\phi;\theta_\gamma,\phi_\gamma) = \frac{3}{2}\{\sin\theta\sin\theta_\gamma\cos(\phi-\phi_\gamma) + \cos\theta\cos\theta_\gamma\cos 2(\phi-\phi_\gamma)\} \tag{106}$$

$$P_{44}(\theta,\phi;\theta_\gamma,\phi_\gamma) = \frac{3}{2}\{\sin\theta\sin\theta_\gamma\cos(\phi-\phi_\gamma) + \cos\theta\cos\theta_\gamma\} \tag{107}$$

$$P_{14} = P_{24} = P_{34} = P_{41} = P_{42} = P_{43} = 0 \tag{108}$$

The phase matrix is identical to the Rayleigh phase matrix of the conventional radiative transfer theory [13–14]. This is because of the small particle assumption and that the pair distribution functions are only correlated for the range of a few diameters.

The boundary condition for the Stokes vector is, from (84)–(89), at $z = 0$

$$\underline{I}(z,\pi-\theta,\phi) = \underline{\underline{R}}(\theta)\underline{I}(z,\theta,\phi) \tag{109}$$

where

$$\underline{\underline{R}}(\theta) = \begin{bmatrix} |R_h(\theta)|^2 & 0 & 0 & 0 \\ 0 & |R_e(\theta)|^2 & 0 & 0 \\ 0 & 0 & \mathrm{Re}(R_h(\theta)R_e^*(\theta)) & -\mathrm{Im}(R_h(\theta)R_e^*(\theta)) \\ 0 & 0 & \mathrm{Im}(R_h(\theta)R_e^*(\theta)) & \mathrm{Re}(R_h(\theta)R_e^*(\theta)) \end{bmatrix} \tag{110}$$

where $R_e(\theta)$ and $R_h(\theta)$ are given by (31) and (32) respectively with $K_z = K\cos\theta$ and $k_z = (k^2 - K^2\sin^2\theta)^{1/2}$.

The dense media radiative transfer equation (95) is to be solved subject to the boundary condition (109). After the solution is calculated, the incoherent Stokes vector that is transmitted back into region 0, $\underline{I}_o(\theta_o, \phi)$, with $\theta_o = \sin^{-1}(K'\sin\theta/k)$ according to Snell's law, is

$$\underline{I}_o(\theta_o, \phi_o) = T(\theta)\underline{I}(z = 0, \theta, \phi) \tag{111}$$

For θ less than critical angle θ_c $(= \sin^{-1}(k/K'))$

$$\underline{\underline{T}}(\theta) = \frac{k^2}{K'^2}$$
$$\begin{bmatrix} 1-|R_h(\theta)|^2 & 0 & 0 & 0 \\ 0 & 1-|R_e(\theta)|^2 & 0 & 0 \\ 0 & 0 & \frac{\cos\theta_o}{\cos\theta}\mathrm{Re}(T_h(\theta)T_e^*(\theta)) & -\frac{\cos\theta_o}{\cos\theta}\mathrm{Im}(T_h(\theta)T_e^*(\theta)) \\ 0 & 0 & \frac{\cos\theta_o}{\cos\theta}\mathrm{Im}(T_h(\theta)T_e^*(\theta)) & \frac{\cos\theta_o}{\cos\theta}\mathrm{Re}(T_h(\theta)T_e^*(\theta)) \end{bmatrix} \tag{112}$$

$T_h(\theta) = 1 + R_h(\theta)$ and $T_e(\theta) = 1 + R_e(\theta)$. For θ greater than the critical angle θ_c, $\underline{\underline{T}}(\theta) = 0$.

The dense media radiative transfer equation (95) with boundary conditions (109)–(110) resemble that of conventional radiative transfer equation of independent scattering except that the expressions for κ_e and $\tilde{\omega}$ are different from those of the conventional theory because of correlated scattering and the fact that the effective propagation constant K has been taken into account. Numerical solutions of the dense media transfer equation follow the same procedure as that of the conventional ones.

5.6 Dense Media Radiative Transfer Equations for Passive Remote Sensing

A classical relation exists between the brightness temperatures of passive remote sensing and the bistatic coefficients of active remote sensing when the medium is of uniform temperature [38]. Recently, an expression has been derived between the two cases when the medium is of nonuniform temperature [11]. The relation is as follows. If $\overline{S}^{(A)}(\bar{r}')$

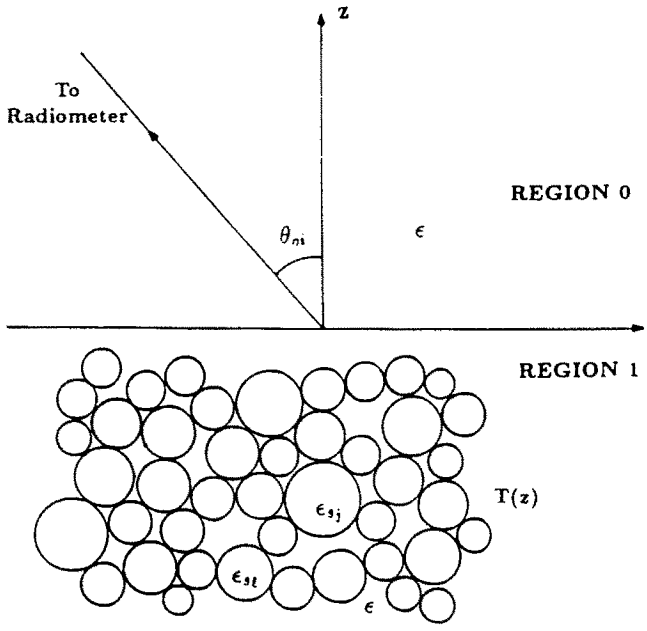

Figure 5.3 Passive remote sensing with a radiometer measuring the thermal emission of a half-space discrete random medium of multiple species in the direction θ_{oi}.

is the Poynting's vector of active remote sensing with incident wave of $\hat{\alpha}$ polarization, $\overline{E}^B(\overline{r})$ is the electric field in passive remote sensing and $T(\overline{r}')$ is the temperature distribution in passive remote sensing, then

$$\lim_{r\to\infty}\int_{\Delta\omega} d\omega \left\langle |\, \hat{\alpha}\cdot\overline{E}^B(\overline{r},\omega)\,|^2 \right\rangle = -\frac{\omega^2\mu^2}{2\pi^3 r^2}\int_{z'<0} d\overline{r}' K_b T(\overline{r}')\,\nabla'\cdot\overline{S}^{(A)}(\overline{r}') \qquad (113)$$

where K_b is Boltzmann's constant and r is the distance between the radiometer and the medium under consideration. Thus the Poynting's vector $\overline{S}^{(A)}(\overline{r})$ can be first calculated in active remote sensing and then the thermal emitted intensity of passive remote sensing can be calculated according to (113). These steps lead to the dense media radiative transfer equations for passive remote sensing.

We consider the problem that the temperature profile $T(z)$ is only a function of z (Fig. 5.3). We can also make use of the azimuthal

symmetry of the problem so that $\mathcal{I}_1$ and $\mathcal{I}_2$ are independent of ϕ and $\mathcal{I}_3 = \mathcal{I}_4 = 0$. Integration over ϕ can also be performed. Thus the dense media radiative transfer equations for passive remote sensing assume the following matrix form of dimension 2, for $0 \leq \theta \leq \pi$, and in region 1,

$$\cos\theta \frac{\partial}{\partial z}\underline{\mathcal{I}}(z,\theta) = -\kappa_e \underline{\mathcal{I}}(z,\theta) + \kappa_e(1-\tilde{\omega})CT(z)\begin{bmatrix}1\\1\end{bmatrix} + \frac{3}{8}\kappa_e\tilde{\omega}\int_0^\pi d\theta' \sin\theta' \underline{\underline{p}}(\theta,\theta')\cdot\underline{\mathcal{I}}(z,\theta') \tag{114}$$

where

$$\underline{\mathcal{I}}(z,\theta) = \begin{bmatrix}\mathcal{I}_1(z,\theta)\\ \mathcal{I}_2(z,\theta)\end{bmatrix} \tag{115}$$

and $\mathcal{I}_1$ is the TM specific intensity and $\mathcal{I}_2$ is the TE specific intensity. Also in (114) $C = K_b K'^2/(\lambda^2 k^2)$, and

$$\underline{\underline{P}}(\theta,\theta') = \begin{bmatrix}p_{11}(\theta,\theta') & p_{12}(\theta,\theta')\\ p_{21}(\theta,\theta') & p_{22}(\theta,\theta')\end{bmatrix} \tag{116}$$

where

$$p_{11}(\theta,\theta') = 2\sin^2\theta\sin^2\theta' + \cos^2\theta\cos^2\theta' \tag{117}$$

$$p_{12}(\theta,\theta') = \cos^2\theta \tag{118}$$

$$p_{21}(\theta,\theta') = \cos^2\theta' \tag{119}$$

$$p_{22}(\theta,\theta') = 1 \tag{120}$$

The boundary conditions for (114) are, for $0 \leq \theta \leq \pi/2$,

$$\mathcal{I}_1(z=0,\pi-\theta) = |R_h(\theta)|^2 \mathcal{I}_1(z=0,\theta) \tag{121}$$

$$\mathcal{I}_2(z=0,\pi-\theta) = |R_e(\theta)|^2 \mathcal{I}_2(z=0,\theta) \tag{122}$$

where $R_h(\theta)$ and $R_e(\theta)$ are TM and TE reflection coefficients respectively and are given by (31) and (32) with $K_z = K\cos\theta$ and $k_z = (k^2 - K^2\sin^2\theta)^{1/2}$.

After (114) is solved subject to the boundary conditions of (121)–(122), the the brightness temperatures in the direction $\theta_o = \sin^{-1}(K'\sin\theta/k)$ for TM and TE polarizations are given by

$$\begin{bmatrix}T_{B1}(\theta_o)\\ T_{B2}(\theta_o)\end{bmatrix} = \frac{1}{C}\begin{bmatrix}(1-|R_h(\theta)|^2)\mathcal{I}_1(z=0,\theta)\\ (1-|R_e(\theta)|^2)\mathcal{I}_2(z=0,\theta)\end{bmatrix} \tag{123}$$

The procedure for numerical solutions of (114), (121)–(122) and (123) is identical to that of conventional radiative transfer theory of independent scattering [9].

5.7 Numerical Illustrations

In this section, we illustrative the numerical results of the dense media radiative transfer equations for active and passive remote sensing. The input physical parameters of the model are the background medium permittivity ϵ, the particles permittivities ϵ_{s_j} and their size distributions as given by a_{s_j}, $n_{s_j}(a_{s_j})$, $s_j = 1, 2, \cdots, L$. Given these physical parameters, all other quantities are calculated. We first calculate the pair distribution functions of multiple species of particles and their Fourier transforms, the effective propagation constant K, the extinction rate κ_e and the effective permittivity $\epsilon_{eff} = K^2/\omega^2\mu$. Besides the effective permittivity, we can also define a mixing formula effective permittivity $\epsilon_{eff}^{(m)}$ which ignores the scattering contribution of (29) that are size dependent as represented by the terms in the square bracket. Thus

$$\epsilon_{eff}^{(m)} = \frac{K_o^2}{\omega^2\mu} \tag{124}$$

where, from (29), K_o obeys the equation

$$K_o^2 = k^2 + \frac{3K_o^2}{D(K_o)} \sum_{s_l=1}^{L} f_{s_l} y_{s_l}(K_o) \tag{125}$$

The albedo $\tilde{\omega}$ is then calculated by using (96). Finally, the dense media radiative transfer equations (95), (109) and (111) for active sensing and (114), and (121)–(123) for passive sensing are solved by using standard numerical procedures of solving transport equations. These will then yield bistatic scattering cross sections for active remote sensing and brightness temperatures for passive remote sensing.

We first compare the results of the dense media radiative transfer equations with those of the conventional radiative transfer equations. The conventional radiative transfer equations are valid for sparse concentration of particles. They assume the same form as in (114)–(123) for passive remote sensing. However, the relations governing the parameters of the conventional transfer equation and the physical parameters

of the medium are based on independent scattering. They are as follows

$$\kappa_e = \kappa_a + \kappa_s \tag{126}$$

$$\kappa_a = \sum_{s_j=1}^{L} \frac{\epsilon''_{s_j}}{\epsilon} \left| \frac{3\epsilon}{\epsilon_{s_j} + 2\epsilon} \right|^2 f_{s_j} k \tag{127}$$

$$\kappa_s = \sum_{s_j=1}^{L} 2 f_{s_j} k^4 a_{s_j}^3 \left| \frac{\epsilon_{s_j} - \epsilon}{\epsilon_{s_j} + 2\epsilon} \right|^2 \tag{128}$$

$$\tilde{\omega} = \frac{\kappa_s}{\kappa_e} \tag{129}$$

$$K' = k \tag{130}$$

and $f_{s_j} = 4\pi n_{s_j} a_{s_j}^3/3$ is the fractional volume occupied by species s_j. It can be verified readily that the dense media parameters reduce to those of (126)–(130) for small fractional volume of f. In terms of numerical results, a major difference between the conventional transfer equations is that the former predict a much larger albedo for the same set of physical parameters of dense media with an appreciable fractional volume. The theoretical predictions of dense medium transport theory have been shown to be in good agreement with controlled laboratory experiments [40]. In Figure 5.4, the results of the brightness temperatures at 18 GHz between the two approaches are compared for a given set of physical parameters that are characteristic of snow. In snow, ice crystals are the particles and the background is air. The fractional volume of ice crystals is usually between 20% and 40% [39]. For the sake of illustration, we have assumed only one species of particles in Fig. 5.4. We have assumed that the ice crystals are spherical. The effects of dense non-spherical particles are a more difficult problem. The presence of scattering prevents the thermal emission from reaching the radiometer giving rise to lower brightness temperatures. Since conventional transfer equations predict a much larger albedo, the calculated brightness temperatures are much lower than those of the dense media radiative transfer equations.

In Figure 5.5, the theoretical results of the dense media transfer equations for one particle species are compared with experimental

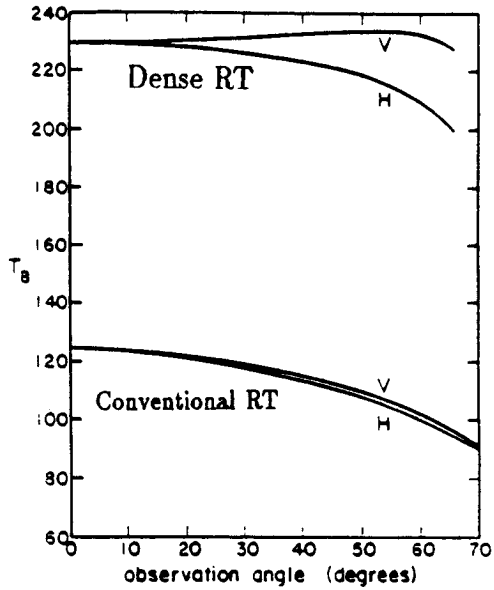

Figure 5.4 Comparison of brightness temperature of vertical V polarization (TM) and horizontal H polarization (TE) as a function of angle θ_o as computed by conventional radiative transfer theory and dense media radiative transfer theory. The input physical parameters are for a half-space medium with one particle species with frequency = 18 GHz, $f_1 = 0.3$, $\epsilon_1 = (3.2 + i0.016)\epsilon_o$, $a_1 = 0.175$ cm, and $T = 272K$. The background medium permittivity is ϵ_o. The calculated mixing formula effective permittivity $\epsilon_{eff}^{(m)}$ is $(1.49 + i0.0029)\epsilon_o$. Parameters represent dry snow.

data of brightness temperature measurements over snow [41–42]. Only the input physical parameters are specified to match the experimental data. A real physical fractional volume of 30% is used in calculating the theoretical result. This is to be contrasted with the conventional theory where sometimes an effective fractional volume is used [42]. The permittivity of particles $\epsilon_s = (3.2 + i0.016)\epsilon_o$ represents typical permittivity of ice in snow and the calculated mixing formula effective permittivity $\epsilon_{eff}^{(m)}$ according to (124)–(125) is $(1.49 + i0.0029)\epsilon_o$ and represents typical permittivity of the overall snow medium. Recent measurements of permittivity of ice have been reported [43]. In Figures 6 to 9, we illustrate the results for media with four species

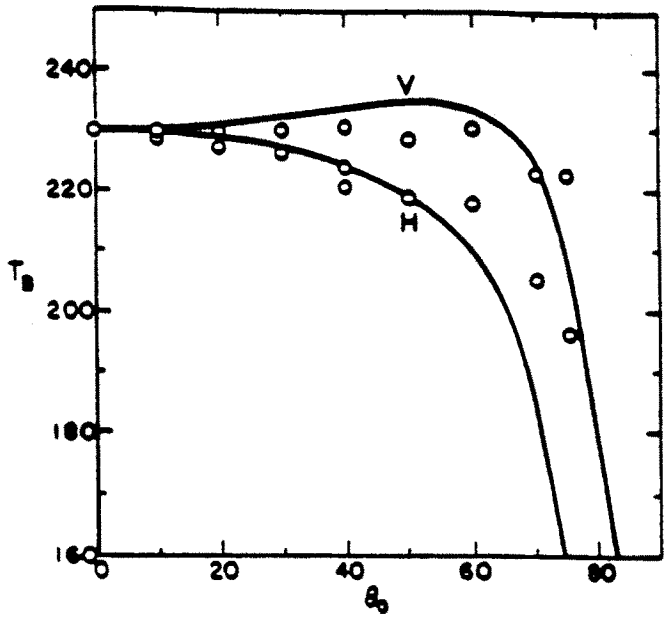

Figure 5.5 Comparison of snow field brightness temperature experimental measurements [41, 42] with theoretical results of dense media radiative transfer equations using the input physical parameters of Fig. 5.4. V stands for vertical polarization and H stands for horizontal polarization.

of particles. In Figure 5.6 the brightness temperatures are illustrated for dry snow with ice particles having four different sizes. There are many more small particles than larger particles. Smaller particles scatter much less than large particles. Hence the scattering induced decrease of brightness temperature is small. Figure 5.7 illustrates the results when there are more large particles. This accounts for a large scattering induced decrease of brightness temperatures. In Figure 5.8, the pair distribution functions as computed by the Percus–Yevick approximation [17–25], for the four particles sizes of Fig. 5.7 are illustrated as a function of particle separation distance. We note that the pair function for the largest particle $g_{44}(r)$ has more oscillations than the other pair functions while $g_{11}(r)$ for the smallest particles has the smallest oscillation. Large oscillations imply less freedom in particle positions. We also note that particle positions are decorrelated when their separations are larger than a few diameters. However as volume

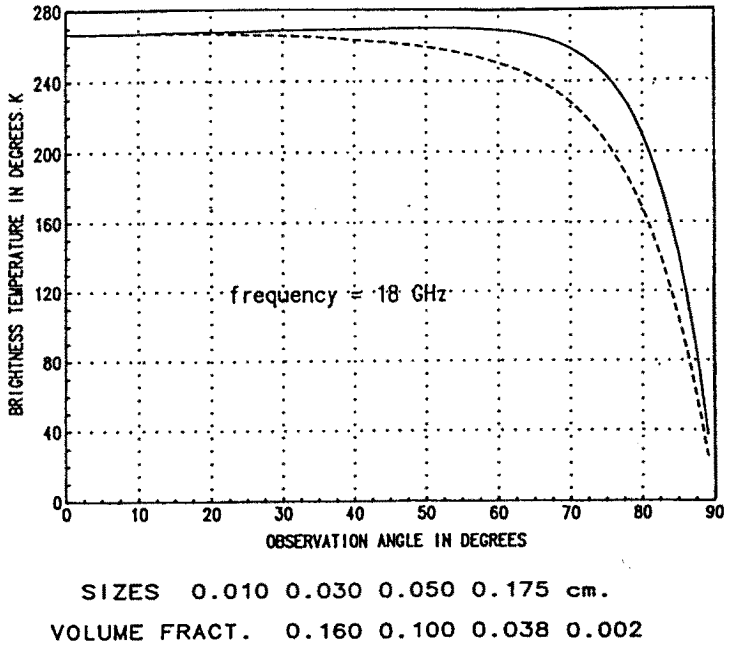

Figure 5.6 Brightness temperature of vertical polarization (solid line) and horizontal polarization (dashed line) as a function of observation angle θ_o at frequency = 18 GHz, for a half-space medium with four species of particles and $T = 272K$. The sizes and fractional volumes are $a_1 = 0.01$ cm, $a_2 = 0.03$ cm, $a_3 = 0.05$ cm, $a_4 = 0.175$ cm, $f_1 = 0.16$, $f_2 = 0.1$, $f_3 = 0.038$, and $f_4 = 0.002$. The permittivity of all the particles is equal to $(3.2 + i0.016)\epsilon_o$. Background medium permittivity is ϵ_o. The calculated mixing formula effective permittivity is $\epsilon_{eff}^{(m)} = (1.49 + i0.0029)\epsilon_o$.

concentration increases, the extent of correlation increases. Thus Fig. 5.8 illustrates the fact that in dense media, large particles have less freedom in positions than small particles. In Figure 5.9, we illustrate the brightness temperatures for media of four particles species with sizes and fractional volumes identical to that of Fig. 5.7. However, in this case, the small particles are water droplets with permittivity ϵ_1 equal to $(20.13 + i31.51)\epsilon_o$ while the other three species are ice particles with $\epsilon_2 = \epsilon_3 = \epsilon_4 = (3.2 + i0.016)\epsilon_o$, we note that the calculated value of mixing permittivity $\epsilon_{eff}^{(m)} = (1.502 + i0.0046)\epsilon_o$. This represents an increase of absorption in the medium and accounts for the increase in brightness temperature of Fig. 5.9 above that of Fig. 5.7. Using the

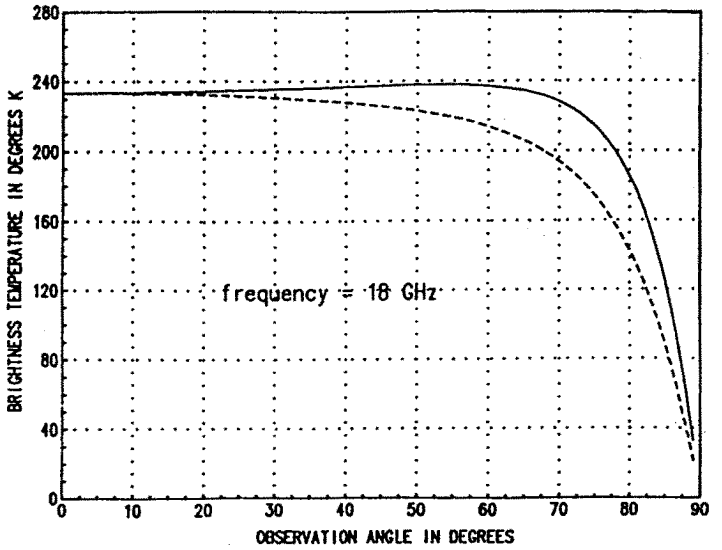

Figure 5.7 Brightness temperature of vertical polarization (solid line) and horizontal polarization (dashed line) as a function of observation angle θ_o at frequency = 18 GHz, for a half-space medium with four species of particles and $T = 272K$. The sizes and fractional volumes are $a_1 = 0.01$ cm, $a_2 = 0.03$ cm, $a_3 = 0.05$ cm, $a_4 = 0.175$ cm, $f_1 = 0.003$, $f_2 = 0.003$, $f_3 = 0.003$, and $f_4 = 0.291$. The permittivity of all the particles is equal to $(3.2 + i0.016)\epsilon_o$. Background medium permittivity is ϵ_o. The calculated mixing formula effective permittivity is $\epsilon_{eff}^{(m)} = (1.49 + i0.0029)\epsilon_o$. Other calculated values are $\kappa_e = 0.0294$ cm^{-1} and $\tilde{\omega} = 0.6374$.

fractional volume of ice crystals and water, and assuming some values of mass densities of ice and water, one can readily calculate the snow mass density and the wetness. In Figure 5.10, we consider the case of a much larger fractional volume of water with $f_1 = 0.05$. This results in a much smaller albedo and a further increase of brightness temperature.

In the studies of remote sensing of geophysical terrain, very often the ground truth data are given in terms of a histogram of particle size distribution. The multiple species model here is applicable to a medium with size distribution. A general expression for particle size distribution is the modified gamma distribution [9]

$$n(a) = K_1 a^P \exp\left(-K_2 a^Q\right) \tag{131}$$

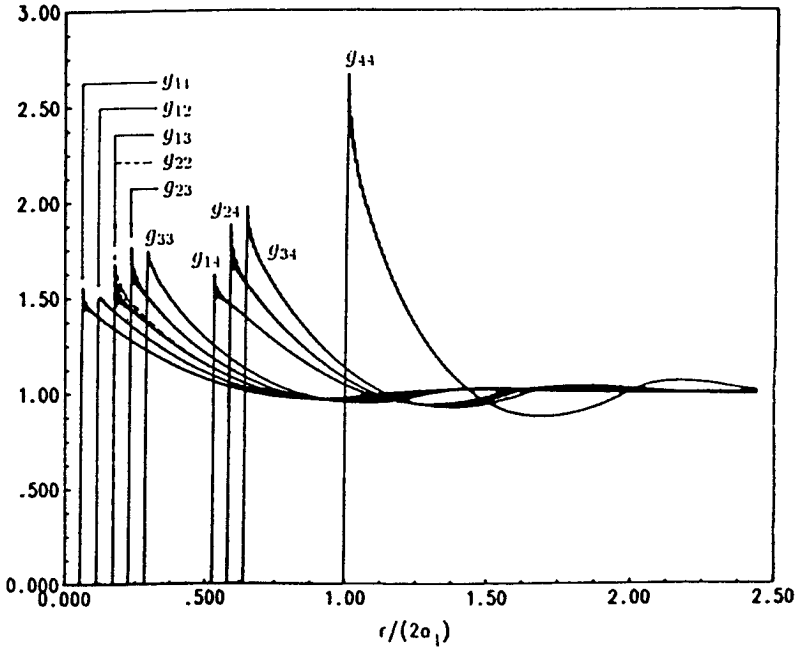

Figure 5.8 Pair distribution functions for the four species of particles of Fig. 7 as a function of separation distance normalized to $2a_4$.

where a is the size of particle and $n(a)da$ gives the number of particles per unit volume having sizes between a and $a + da$.

The modified gamma distribution defined in (131) is a four-parameter distribution function. The four constants K_1, P, K_2, and Q are positive and real. The behavior of this distribution function for small size is governed by the power law of a^P, and for large a, $\exp\left(-K_2 a^Q\right)$ contains the dropoff at large particle size. The normalizing factor K_1 is mainly dependent on the total fractional volume f_{tot} occupied by particles. This is obtained by multiplying $n(a)$ by $4\pi a^3/3$ and integrating over the entire range of size (from 0 to ∞)

$$f_{tot} = \frac{4\pi}{3} \frac{K_1}{Q} K_2^{-\frac{P+4}{Q}} \Gamma\left(\frac{P+4}{Q}\right) \tag{132}$$

where Γ is gamma function. The parameter K_2 is related to the mode size a_c at which $n(a_c)$ is a maximum in the distribution. The mode radius a_c can be found by setting the derivative of (131) with respect

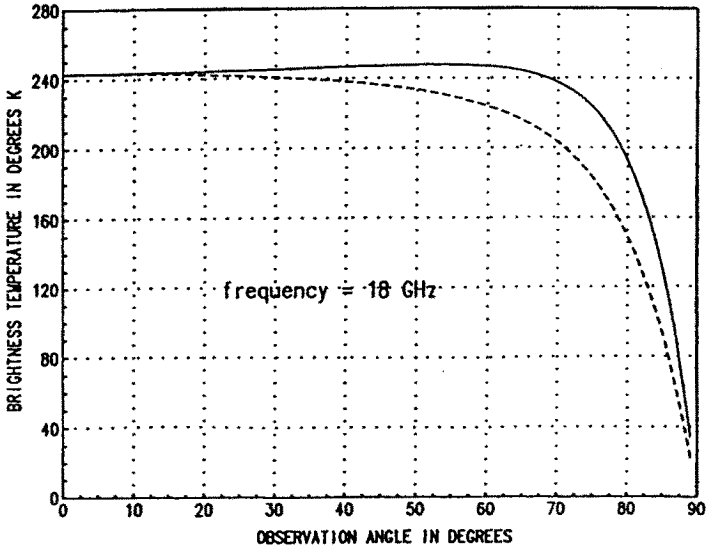

Figure 5.9 Brightness temperature of vertical polarization (solid line) and horizontal polarization (dashed line) as a function of observation angle θ_o at frequency = 18 GHz, for a half-space medium with four species of particles and $T = 272K$. The sizes and fractional volumes are $a_1 = 0.01$ cm, $a_2 = 0.03$ cm, $a_3 = 0.05$ cm , $a_4 = 0.175$ cm, $f_1 = 0.003$, $f_2 = 0.003$, $f_3 = 0.003$, and $f_4 = 0.291$. However the permittivities are different. The smallest particles are water with $\epsilon_1 = (20.13 + i31.51)\epsilon_o$ (at 18 GHz). The other species are ice particles with $\epsilon_2 = \epsilon_3 = \epsilon_4 = (3.2 + i0.016)\epsilon_o$. Background medium permittivity is ϵ_o. The calculated values are: mixing formula effective permittivity $\epsilon_{eff}^{(m)} = (1.502 + i0.0046)\epsilon_o$, $\tilde{\omega} = 0.0345$ cm^{-1}, $\tilde{\omega} = 0.537$.

to a equal to zero.

$$a_c = \left(\frac{P}{K_2 Q}\right)^{\frac{1}{Q}} \tag{133}$$

One may construct a great variety of specific distributions based on the general formula (131). Usually, the constants P and Q can be fitted empirically to the slopes of an experimentally obtained particle size distribution. Instead of using K_1, K_2, P and Q to characterize the distribution, we will use f_{tot}, a_c, P and Q.

In Figures 11 and 12, we plot the brightness temperatures for a

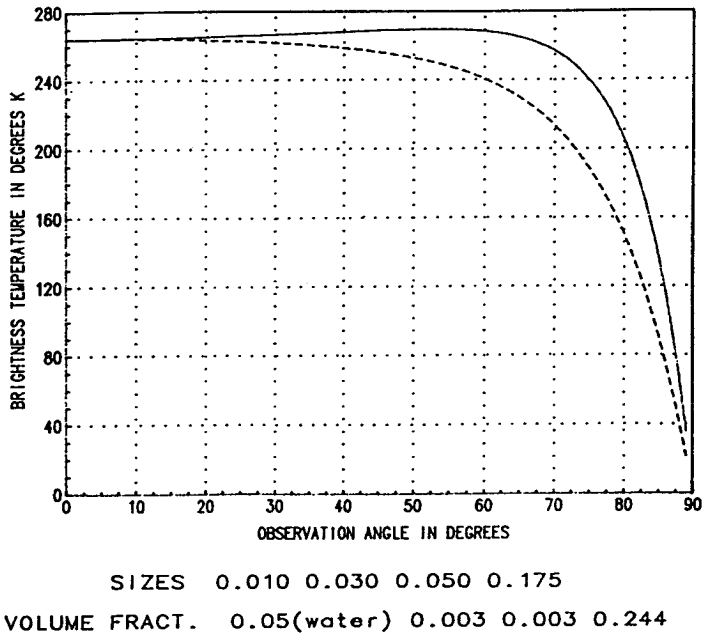

Figure 5.10 Brightness temperature of vertical polarization (solid line) and horizontal polarization (dashed line) as a function of observation angle θ_o at frequency = 18 GHz, for a half space medium with four species of particles and $T = 272K$. The sizes and permittivities are as in Fig. 5.9. Fractional volumes are different with $f_1 = 0.05$, $f_2 = 0.003$, $f_3 = 0.003$, $f_4 = 0.244$. The calculated values are: $\epsilon_{eff}^{(m)} = (1.704+i0.0449)\epsilon_o$, $\kappa_e = 0.151\ \text{cm}^{-1}$, and $\tilde{\omega} = 0.114$.

half space medium with particles obeying a gamma size distribution for two different mode radii of 0.075 cm and 0.1 cm respectively. The permittivity of the particles is $\epsilon_s = (3.2+i0.002)\epsilon_o$ with a smaller loss tangent than previous figures. From the figures, it can be seen that the larger particles which correspond to the tail of the gamma size distribution can contribute significantly to scattering and scattering induced decreasing of brightness temperatures. Figure 5.12 has a lower brightness temperature than Fig. 5.11 because of a larger mode radius.

Generally, a large P and Q correspond to a narrow size distribution with a small standard deviation. In Figures 12, 13, 14, 15, we illustrate respectively the size distributions, the extinction rate κ_e, the effective real dielectric constant ($=\text{Re}(K^2/k^2)$) and the albedo for two size distributions of particles: (a) $P=2$, $Q=2$, $a_c=0.0875$ cm,

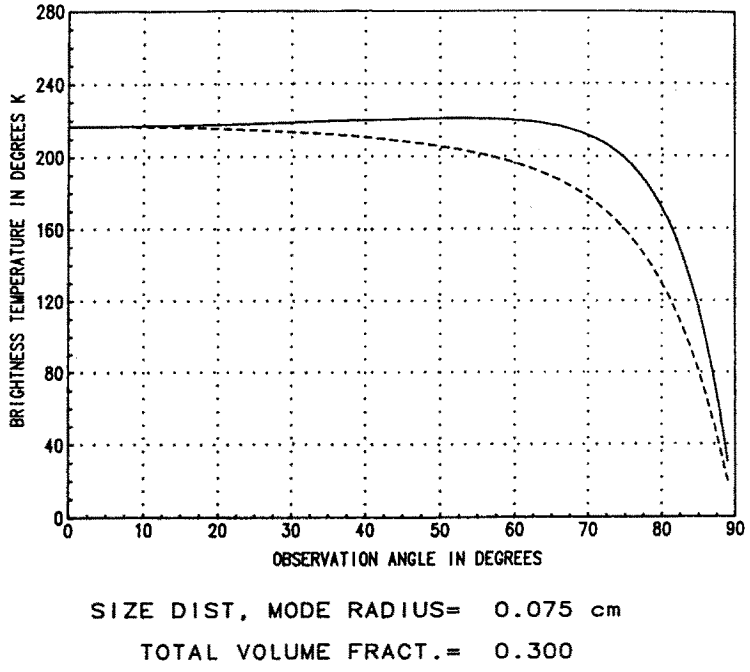

Figure 5.11 Brightness temperature of vertical polarization (solid line) and horizontal polarization (dashed line) as a function of observation angle θ_o at frequency = 18 GHz, for a half-space medium with a gamma size distribution of particles with $P = 6$, $Q = 2$, $a_c = 0.075$ cm, $f_{tot} = 0.3$, $\epsilon_s = (3.2 + i0.002)\epsilon_o$ and $T = 272K$. The computed values are: effective propagation constant $K = (4.60 + i0.2865 \times 10^{-2})$ cm^{-1}, $\kappa_e = 0.00573$ cm^{-1}, and $\tilde{\omega} = 0.7573$.

and (b) $P=12$, $Q=20$, $a_c=0.175$ cm.

Thus particles in distribution (a) are governed by a broad size distribution with a small mode radius of 0.0875 cm. The particles in distribution (b) are governed by a narrow size distribution with a much larger mode radius of 0.175 cm . The extinction rate in Fig. 5.14 contains some interesting features. For small fractional volume, (b) has a larger scattering attenuation rate than (a), because for small fractional volume particles scatter independently and larger particles scatter more. However at large fractional volume, (a) has larger extinction rate than (b) because (a) becomes more homogeneous at large fractional volume. On the other hand (b) has a sufficient amount of large particles that exist in the tail of the gamma size distribution and they contribute significantly to scattering attenuation. On the other hand,

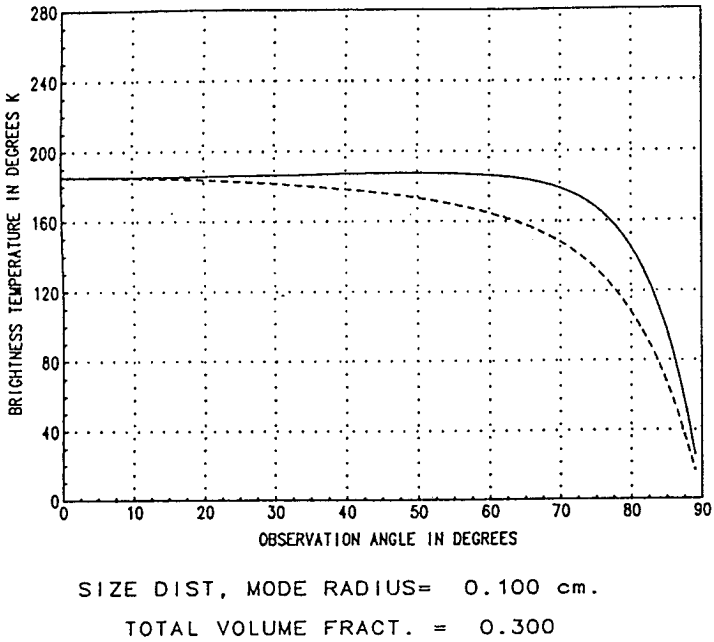

Figure 5.12 Brightness temperature of vertical polarization (solid line) and horizontal polarization (dashed line) as a function of observation angle θ_o at frequency = 18 GHz, for a half-space medium with a gamma size distribution of particles with $P = 6$, $Q = 2$, $a_c = 0.1$ cm, $f_{tot} = 0.3$, $\epsilon_s = (3.2 + i0.002)\epsilon_o$ and $T = 272K$. The computed values are: effective propagation constant $K = (4.60 + i0.584 \times 10^{-2})$ cm^{-1}, $\kappa_e = 0.0117$ cm^{-1}, and $\tilde{\omega} = 0.881$.

Fig. 15 shows that the real parts of the effective dielectric constants are indistinguishable between (a) and (b). Figure 5.16 shows that the albedo of (b) is larger than (a) for small fractional volume and vice versa for large fractional volume. Figure 5.14 shows that (a) is closer to "independent scattering" than (b) because the peak is broader and occurs at a larger fractional volume than (b).

In Figure 5. 17, we compare the result of backscattering coefficient in active remote sensing with experimental data at 17 GHz. The parameters are a two layer medium with the uppermost layer being air. The middle layer is a slab of scatterers with $\epsilon_s = (3.2 + i0.002)\epsilon_o$ of thickness $d = 27$ cm overlying the lowermost layer of a homogeneous half-space of $\epsilon_2 = (6 + i0.6)\epsilon_o$. The particles in the scattering layer obey gamma size distribution with $P = 6$, $Q = 2$ and $a_c = 0.125$ cm.

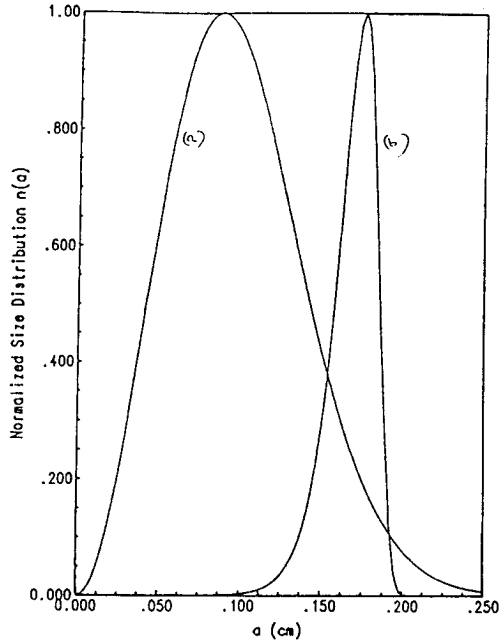

Figure 5.13 Normalized size distribution for two size distributions (the maximum of number densities is normalized to 1). (a) $P = 2$, $Q = 2$, $a_c = 0.0875$ cm, $f_{tot} = 0.35$, (b) $P = 12$, $Q = 20$, $a_c = 0.175$ cm, $f_{tot} = 0.35$.

The backscattering coefficient is calculated by solving (95) subject to boundary conditions at the top and the lower boundary. The backscattering coefficient $\sigma = 4\pi \cos\theta_{oi} \mathcal{I}_o(\theta_{oi}, \pi + \phi_{oi})$ for HH polarization is illustrated in Fig. 5.16 as a function of incidence angle θ_{oi}. The data has been matched before [40] based on a single particle size model with $a = 0.175$ cm. Figure 5.17 shows that by using a broad size distribution with $P = 6$, $Q = 2$, one can achieve a reasonable match with a smaller mode radius of $a_c = 0.125$ cm.

5.8 Conclusions

In this chapter, the dense media radiative transfer equations are derived for discrete random media with multiple species of small particles. Multiple species refers to the case when the medium is a mixture of particles with multiple sizes and permittivities. This is often the case in geophysical terrain, composite and heterogeneous materials. Unlike

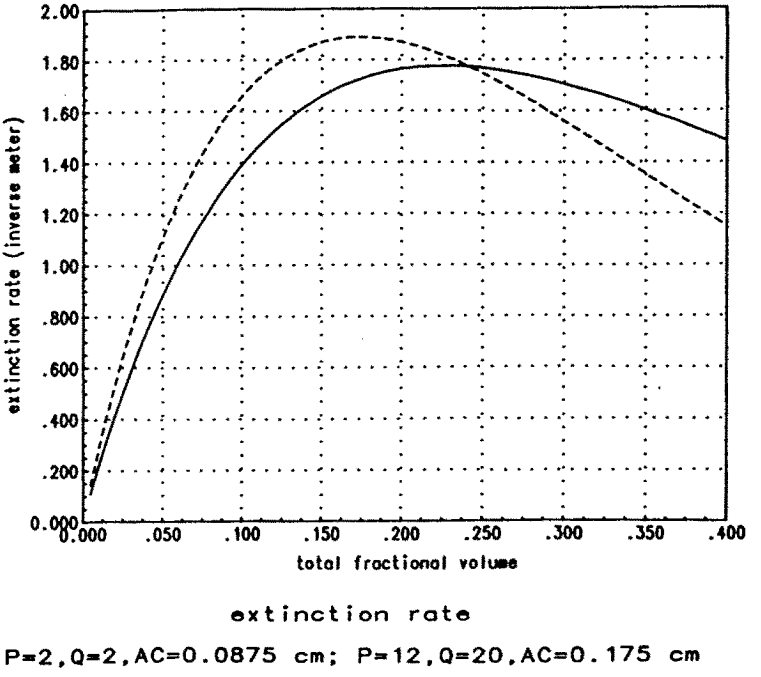

Figure 5.14 Extinction rate as a function of total fractional volume for two size distributions: (a) (solid line) $P = 2$, $Q = 2$, $a_c = 0.0875$ cm, and (b) (dashed line) $P = 12$, $Q = 20$, $a_c = 0.175$ cm. For both cases $\epsilon_s = (3.2 + i0.002)\epsilon_o$, frequency = 17 GHz.

the conventional radiative transfer theory which is derived heuristically, the dense media radiative transfer equations are based on analytic wave theory by making the quasicrystalline approximation with coherent potential on the mass operator and the ladder approximation of correlated scatterers on the intensity operator. Correlated scattering between different particles is taken into account. The pair distribution functions of correlated particle positions of multiple species are calculated by using the Percus–Yevick equation of non-interpenetrable spheres. We have also illustrated the dense media radiative transfer theory for applications to active and passive remote sensing.

The dense medium radiative transfer theory has been used to explain the phenomena observed in a controlled laboratory experiment [5,40,44]. In the controlled laboratory experiment, it is possible to make incremental changes in particle concentrations and measure subsequent scattering properties of the medium. The experimental data indicate that, in a dense medium with small particles, both the coherent atten-

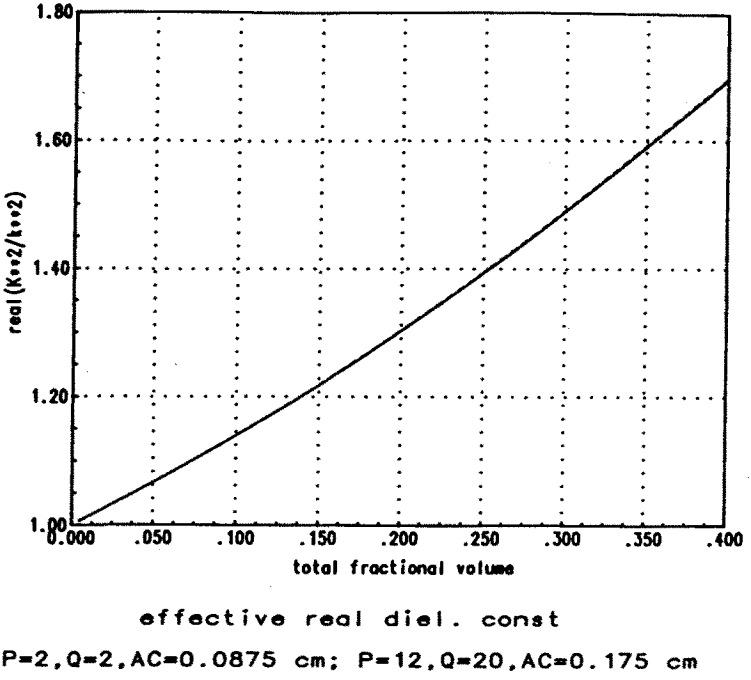

Figure 5.15 Effective real dielectric constant defined as $\mathrm{Re}(K^2/k^2)$ as a function of total fractional volume for two size distributions: (a) (solid line), (b) (dashed line). Parameters are the same as in Fig. 14.

uation rates and bistatic intensities increase with the volume fraction of the particles until a maximum is reached, and then decrease when the volume fraction further increases. Thus the attenuation rate and the bistatic scattering exhibit a peak as a function of concentration of particles. The magnitudes of both are also less than those predicted by independent scattering assumption and the conventional radiative transfer theory. This is the laboratory experimental results observed for small particles. (For particles larger than a wavelength, the laboratory experimental observed scattering can be larger than conventional transfer theory [5]. However, this is usually not the case in microwave remote sensing of snow.) These phenomena cannot be explained by the conventional radiative transfer theory. On the other hand, it has been shown that the dense medium radiative transfer theory is in agreement with these experimental features [40].

Although we have only illustrated the results for active and passive remote sensing of snow media, the theory can be readily applied

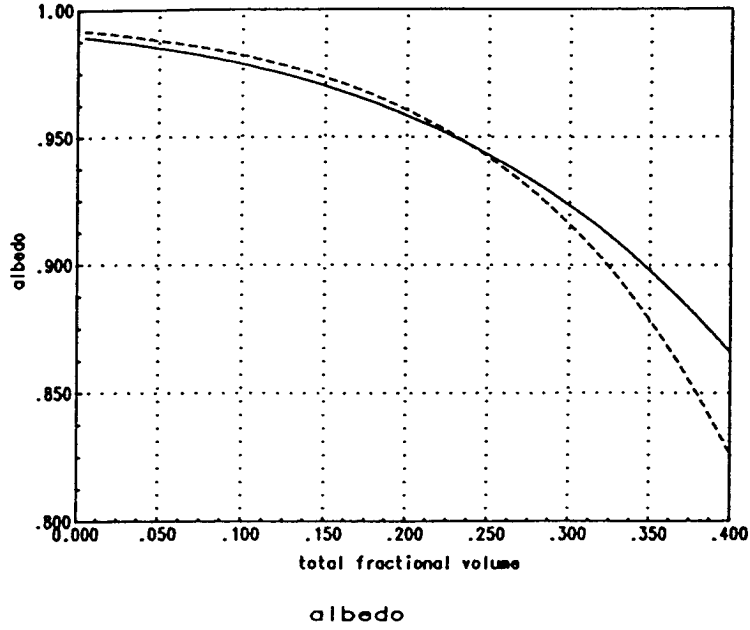

Figure 5.16 Albedo as a function of total fractional volume for two size distributions: (a) (solid line), (b) (dashed line). Parameters are the same as in Fig. 5.14.

to other geophysical terrain with dense distribution of particles as well as to heterogeneous composite materials with multiple species of particles such as carbon-resin matrix. The basic limitation of the theory at present is that the particles have been assumed to be spherical. Studies of non-spherical particles of a single species have been treated elsewhere [45,46].

It is also important to note that the ladder approximation does not include cyclical scattering processes that contribute directly to backscattering enhancement [44,47–55].

In this chapter we have used the Percus–Yevick approximation to calculate the pair distribution functions of a medium consisting of particles with a size distribution. The Percus–Yevick approximation was originally used for studying pair functions of liquid molecules. We have used a special case of Percus–Yevick approximation assuming that the particles are non-interpenetrable and there are no inter-particle forces. It has been shown that the Percus–Yevick pair function agrees well with that of the laboratory samples of small glass spheres embedded

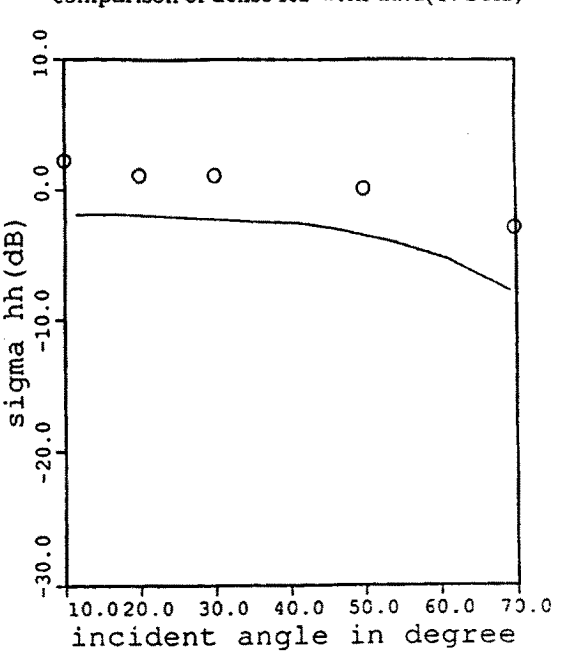

Figure 5.17 Comparison of dense medium radiative transfer theory with backscattering data from snow. The input parameters are frequency = 17 GHz, $\epsilon_s = (3.2 + i0.002)\epsilon_o$, d = layer thickness = 27 cm, ϵ_2 = permittivity of homogeneous half-space below scattering layer = $(6 + i0.6)\epsilon_o$. The gamma size distribution parameters are $P = 6$, $Q = 2$, $a_c = 0.125$ cm, and $f_{tot} = 0.2$. Based on these input parameters, the computed values are $K = (4.064 + i0.00941)\text{cm}^{-1}$, $\kappa_e = 0.0188\text{cm}^{-1}$, and $\tilde{\omega} = 0.961$.

in a styrofoam medium [56].

References

[1] Twersky, V., "Coherent scalar field in pair-correlated random distributions of aligned scatterers," *J. Math. Phys.*, **18**, 2468–2486, 1977.

[2] Tsang, L., and J. A. Kong, "Multiple scattering of electromagnetic waves by random distribution of discrete scatterers with coherent potential and quantum mechanical formalism," *J. Appl. Phys.*,

51, 3465–3485, 1980.

[3] Shin, R. T., and J. A. Kong,"Radiative transfer theory for active remote sensing of homogeneous layer containing spherical scatterers," *J. Appl. Phys.*, **52**, 4221–4230, 1981.

[4] Tsang, L., and J. A. Kong, "Effective propagation constants for coherent electromagnetic wave propagation in media embedded with dielectric scatterers," *J. Appl. Phys.*, **53**, 7162–7173, 1982.

[5] Ishimaru, A., and Y. Kuga, "Attenuation constant of a coherent field in a dense distribution of particles," *J. Opt. Soc. Am.*, **72**, 1317–1320, 1982.

[6] Tsang, L., and J. A. Kong, "Scattering of electromagnetic waves from a half space of densely distributed dielectric scatterers," *Radio Science*, **18**, 1260–1272, 1983.

[7] Lang, R. M., and J. S. Sidhu, "Electromagnetic backscattering from a layer of vegetation: a discrete approach," *IEEE Trans. Geosci. Remote Sensing*, **21**, 62–71, 1983.

[8] Varadan, V. K., V. N. Bringi, V. V. Varadan, and A. Ishimaru, "Multiple scattering theory for waves in discrete random media and comparison with experiments," *Radio Science*, **18**, 321–327, 1983.

[9] Tsang, L., J. A. Kong, and R. T. Shin, *Theory of Microwave Remote Sensing*, Wiley-Interscience, New York, 1985.

[10] Tsang, L., and A. Ishimaru, "Radiative wave equations for vector electromagnetic propagation in dense nontenuous media," *J. of Electro. Waves Applic.*, **1**, 59–72, 1987.

[11] Tsang, L., "Passive remote sensing of dense nontenuous media," *J. of Electro. Waves Applic.*, **1**, 159–173, 1987.

[12] Zhu, P. A., A. K. Fung, and K. W. Wong, "Effective propagation constants in dense random media under effective medium approximation," *Radio Science*, **22**, 234–250, 1987.

[13] Chandrasekhar, S., *Radiative Transfer*, Dover, New York, 1960.

[14] Ishimaru, A., *Wave Propagation and Scattering in Random Media*, **1**, **2**, Academic Press, New York, 1978.

[15] Tsang, L., and A. Ishimaru, "Radiative wave and cyclical transfer equation for dense nontenuous media," *J. Opt. Soc. Am. A*, **2**,

2187–2194, 1985.

[16] Tsolakis, A. I., I. M. Besieris, and W. E. Koher, "Two-frequency radiative transfer equation for scalar wave in random distribution of discrete scatterers with pair correlations," *Radio Science,* **20**, 1037–1052, 1985.

[17] Ding, K. H., and L. Tsang, "Effective propagation constants in media with densely distributed dielectric particles of multiple sizes and permittivities," in *Progress in Electromagnetics Research* **1**, J. A. Kong, ed., Elsevier, New York, Ch. 3, 241–295. 1989.

[18] Ding, K. H., and L. Tsang, "Effective propagation constants of dense nontenuous media with multi-species of particles," *J. of Electro. Waves Applic.*, **2**, 757–777, 1988.

[19] Wertheim, M. S., "Exact solution of the Percus-Yevick integral equation for hard spheres," *Phys. Rev. Lett.*, **20**, 321–323, 1963.

[20] Lebowitz, J. L., "Exact solution of generalized Percus-Yevick equation for a mixture of hard spheres," *Phys. Rev.*, **133**, A895–899, 1964.

[21] Wertheim, M. S., "Analytic solution of the Percus-Yevick equation," *J. Math. Phys.*, **5**, 643–651, 1964.

[22] Baxter, R. J., "Ornstein-Zernike relation for a disordered fluid," *Aust. J. Phys.*, **21**, 563–569, 1968.

[23] Baxter, R. J., "Ornstein-Zernike relation and Percus-Yevick approximation for fluid mixtures," *J. Chem. Phys.*, **52**, 4559–4562, 1970.

[24] Leonard, P. J., D. Henderson, and J. A. Barker, "Calculation of the radial distribution function of hard-sphere mixtures in the Percus-Yevick approximation," *Molec. Phys.*, **21**, 107–111, 1971.

[25] Waseda, Y., *The Structure of Non-Crystalline Materials, Liquids and Amorphous Solids*, McGraw-Hill, New York, 1980.

[26] Winebrenner, D., L. Tsang, B. Wen, and R. West, "Sea ice characterization measurements needed for testing of microwave remote sensing models," *IEEE Trans. on Oceanic Engineering,* **14**, 149–158, 1988.

[27] Frisch, V., "Wave propagation in random medium," in *Probabilistic Methods in Applied Mathematics,* **1**, A. T. Bharucha-Reid, ed.,

Academic Press, New York, 1968.

[28] Rosenbaum, S., "The mean Green's function: A nonlinear approximation," *Radio Science,* **6**, 379–386, 1971.

[29] Dence, D., and J. E. Spence, "Wave propagation in random anisotropic media," in *Probabilistic Methods in Applied Mathematics,* **3**, A. T. Bharucha-Reid, ed., Academic Press, New York, 1973.

[30] Soven, P., "Coherent-potential model of substitutional disordered alloys," *Phys. Rev.,* **156**, 809–813, 1967.

[31] Gyorffy, B. L., "Electronic states in liquid metals: A generalization of the coherent–potential approximation for a system with short-range order," *Phys. Rev. B.,* **1**, 3290–3299, 1970.

[32] Korringa, J., and R. L. Mills, "Coherent potential approximation for random systems with short range correlations," *Phys. Rev. B.,* **5**, 1654–1655, 1972.

[33] Kohler, W. E., and G. C. Papanicolaou, "Some applications of the coherent potential approximation," in *Multiple Scattering and Waves in Random Media,* P. L. Chow, W. K. Kohler, and G. C. Papanicolaou, eds., North-Holland, New York, 199–223, 1981.

[34] Papanicolaou, G., and R. Burridge, "Transport equations for the Stokes parameters from Maxwell equations in a random medium," *J. Math. Physics,* **16**, 2074–2085, 1975.

[35] Tsang, L., and J. A. Kong, "Wave theory for microwave remote sensing of a half-space random medium with three-dimensional variations," *Radio Science,* **14**, 359–369, 1979.

[36] Zuniga, M. A., and J. A. Kong, "Modified radiative transfer for a two-layer random medium," *J. Appl. Phys.,* **51**, 5228–5244, 1980.

[37] Fante, R. L., "Relation between radiative-transport theory and Maxwell's equations in dielectric media," *J. Opt. Soc. Am.,* **71**, 460–468, 1981.

[38] Peake, W. H., "Interaction of electromagnetic waves with some natural surfaces," *IEEE Trans. Ant. Prop.,* **AP-7**, Special Supplement, S324–S329, 1959.

[39] Ulaby, F. T., R. K. Moore, and A. K. Fung, *Microwave Remote Sensing: Active and Passive,* **1, 2, 3**, Artech-House, Reading, MA, 1986.

[40] Wen, B., L. Tsang, D. P. Winebrenner, and A. Ishimaru, "Dense medium radiative transfer theory: comparison with experiment and application to microwave remote sensing and polarimetry," *IEEE Trans. Geosci. Remote Sensing*, **28**, 46–59, Jan. 1990.

[41] Shiue, J. C., A. T. C. Chang, H. Boyne, and D. Ellerbruch, "Remote sensing of snowpack with microwave radiometers for hydrologic applications," *Proc. 12th International Symposium of Remote Sensing and Environment*, **2**, 877–886, University of Michigan, Ann Arbor, Michigan, 1978.

[42] Kong, J. A., R. T. Shin, J. C. Shiue, and L. Tsang, "Theory and experiment for passive remote sensing of snowpacks," *J. Geophys. Res.*, **84**, 5669–5673, 1979.

[43] Matzer, C. and J. Wegmueller, "Dielectric properties of fresh water ice at microwave frequencies," *J. Phys. D: Appl. Phys.*, **20**, 1623–1630, 1987.

[44] Kuga, Y., and A. Ishimaru, "Retroreflectance from a dense distribution of spherical particles," *J. Opt. Soc. Am. A.*, **1**, 831–835, 1984.

[45] Tsang, L., "Thermal emission of nonspherical particles," *Radio Science*, **19**, 966–974, 1984a.

[46] Tsang, L., "Scattering of electromagnetic waves from a half space of nonspherical particles," *Radio Science*, **19**, 1450–1460, 1984b.

[47] Barabannenkov, Y. N., "Wave corrections to transfer equation for backscattering," *Izv. Vyssh. Uchebn. Zaved. Radiofiz.*, **16**, 88–94, 1973.

[48] Tsang, L., and A. Ishimaru, "Backscattering enhancement of random discrete scatterers," *J. Opt. Soc. Am. A.*, **1**, 836–839, 1984.

[49] Albada, M. P., and A. Langendijk, "Observation of weak localization of light in a random medium," *Phys. Rev. Lett.*, **55**, 2692–2695, 1985.

[50] Wolf, P. E., and G. Maret, "Weak localization and coherent backscattering of photons in disordered media," *Phys. Rev. Lett.*, **55**, 2696–2699, 1985.

[51] Tsang, L., and A. Ishimaru, "Radiative wave and cyclical transfer equations for dense nontenuous media," *J. Opt. Soc. Am. A.*, **2**,

2187–2194, 1985.

[52] Tsang, L., and A. Ishimaru, "Theory of backscattering enhancement of random discrete isotropic scatterers based on the summation of all ladder and cyclical terms," *J. Opt. Soc. Am. A.*, **2**, 1331–1338, 1985.

[53] Ishimaru, A., and L. Tsang, "Backscattering enhancement of random discrete scatterers of moderate sizes," *J. Opt. Soc. Am. A.*, **5**, 228–236, 1988.

[54] van der Mark, M. B., M. P. van Albada, and A. Lagendijk, "Light scattering in strongly scattering media: Multiple scattering and weak localization," *Phys. Rev. B.*, **37**, 3575–3592, 1988.

[55] You, K. M., Y. Takiguchi, and R. R. Alfano, "Weak localization of photons: contributions from the different scattering path lengths," *IEEE Photonics Technology Letters*, **1**, 94–96, 1989.

[56] Mandt, C. E., *Microwave propagation and scattering in a dense distribution of spherical particles*, M.S. thesis, University of Washington, 1987.